

NASA CONTRACTOR REPORT

NASA CR-61080

GPO PRICE \$ _____

CSFTI PRICE(S) \$ _____

Hard copy (HC) 3.00

Microfiche (MF) .50

ff 653 July 65

NASA CR-61080

FACILITY FORM 608

N 65-32960

(ACCESSION NUMBER)

(THRU)

50

(PAGES)

1

(CODE)

CR-61080

(NASA CR OR TNX OR AD NUMBER)

20

(CATEGORY)

MESOSCALE STRUCTURE OF 11-20 KM WINDS

Prepared Under Contract NAS8-5294 by

A. I. Weinstein and E. R. Reiter

METEOROLOGY RESEARCH, INCORPORATED
Altadena, California

For

NASA - GEORGE C. MARSHALL SPACE FLIGHT CENTER
Huntsville, Alabama

June 28, 1965

MESOSCALE STRUCTURE OF 11-20 KM WINDS

By

A. I. Weinstein and E. R. Reiter

**Prepared Under Contract NAS8-5294 by
METEOROLOGY RESEARCH, INCORPORATED
Altadena, California**

**For
Aero-Astroynamics Laboratory**

**Distribution of this report is provided in the interest of
information exchange. Responsibility for the contents
resides in the author or organization that prepared it.**

NASA - GEORGE C. MARSHALL SPACE FLIGHT CENTER

FOREWORD

This report presents further results of a study conducted by Meteorology Research, Inc., Altadena, California as part of NASA Contract NAS8-5294 with the Aerospace Environment Office, Aero-Astrodynamics Laboratory, NASA-George C. Marshall Space Flight Center, Huntsville, Alabama. The NASA contract monitor was Mr. James R. Scoggins; Mr. Alan I. Weinstein, Meteorology Research, Inc., and Dr. Elmar R. Reiter, Colorado State University were principal investigators.

The initial part of the study was published as NASA TMX-53115, August 1964, and was concerned primarily with individual velocity profiles measured on separate days and with two series of profiles approximately one hour apart. The initial study confirmed the fact that series of profiles are more valuable than individual ones in developing theories to explain the characteristics of the observed small-scale motions. Thus the present report is confined to an analysis of eleven series of velocity profiles measured at the Western Test Range.

This report concludes Contract NAS8-5294. The contract period covered by this report was April 1964 to April 1965.

ACKNOWLEDGMENTS

The data used in this study were supplied by Mr. James R. Scoggins, George C. Marshall Space Flight Center, Huntsville, Alabama. The authors wish to thank Dr. P. B. MacCready, Jr., and Dr. T. B. Smith of Meteorology Research, Inc., and Dr. J. R. Stinson of the Navy Weather Research Facility, Norfolk, Virginia, for their valuable suggestions during the course of the investigation.

TABLE OF CONTENTS

	Page
SUMMARY	1
I. INTRODUCTION	3
II. GENERAL CHARACTERISTICS	4
III. DATA SUMMARY	9
IV. MODELS OF MESOSCALE FLOW	11
V. EFFECTS OF QUASI-INERTIAL OSCILLATIONS ON WIND PROFILES	18
VI. EVIDENCE IN SUPPORT OF THE QUASI-INERTIAL OSCILLATION MODEL	21
VII. POTENTIAL CAUSES OF QUASI-INERTIAL OSCILLATIONS	26
VIII. FORECASTING APPLICATION	28
IX. CONCLUSIONS AND RECOMMENDATIONS FOR FUTURE RESEARCH	34
Appendix A. Tables of Percentage Frequency of Occurrence of Shears and the Depths Through Which They Were Active	36
Appendix B. Joint Empirical Probability Distribution of Wind Speed Change (ΔV) and Depth of the Change Layer (ΔZ)	38
REFERENCES	40

LIST OF ILLUSTRATIONS

Figure	Title	Page
1.	Speed and Direction Profiles, 12-13 December 1963	5
2.	Common Changes in Mesoscale Perturbations	8
3.	Smoothed Joint Empirical Probability Distribution of Wind Speed Change (ΔV) and Depth of the Layer (ΔZ) (Probability in per cent of total observations - 2088) . . .	10
4.	Spherical Balloon Tracks, 26-27 December 1963	12
5.	Speed and Direction Profiles, 26-27 December 1963 . . .	14
6.	Velocity Variation Through an Inertial Cycle	18
7.	Illustrative Model of Stacked Quasi-Inertial Oscillations .	19
8.	Speed, Direction, Temperature, and Ri Profiles	22
9.	Wind Speed and Direction Profiles, 2139Z, 28 January 1964	24
10.	Plot of Amplitude (ΔV_{\max}) vs. Vertical Wavelength (λ_V) for Vertical Oscillations at the Maximum Development .	29
11.	Forecast Nomogram	30
12.	Frequency Distribution of Shear Strengths	32

MESOSCALE STRUCTURE OF 11-20 KM WINDS

SUMMARY

The tracking of spherical superpressure balloons by an FPS-16 radar located off the coast of Southern California, near Point Mugu, has generated eleven series of wind speed and direction profiles which attained a degree of vertical resolution far greater than that of standard GMD-1 profiles. Each series contained from eight to eleven individual pairs of wind speed and direction profiles spaced over a period of time from 8-12 hours. This report contains an evaluation of these data, and also draws partially on other comparable soundings from California and Florida. The analysis is concentrated in the 11-20 km altitude range and conditions inferred may or may not be applicable elsewhere.

Every profile in each series contained mesoscale perturbations of 5 to 10 m/s, and 5 to 20 degrees over a vertical depth up to 2 km, which persisted in recognizable form at approximately the same altitude throughout the series. Often the magnitude of a perturbation changed by as much as 50 per cent, but only rarely did the depth change by more than 10 per cent.

Several models of mesoscale flow, suggested to explain wind fluctuations similar to those of the present study, are critically examined. The model which appears most suitable pictures the wind regime as the result of the relative horizontal motion of stacked layers of large horizontal extent. The layers have sufficient stability so they operate relatively independently. Motion within each layer is controlled principally by a quasi-inertial oscillation around the basic geostrophic flow at that level. The vertical shears arise in part because the inertial oscillation amplitude and phase of one layer are not correlated to the amplitude and phase at other layers. The shear magnitudes slowly evolve as the phases evolve. The maximum possible shears are limited by the local thermal stability through a Richardson's number criterion.

The concepts of the above model are combined with a statistical evaluation of the wind speed profiles series to arrive at a suggested method of forecasting maximum wind shears that might evolve from a

given wind speed profile in the altitude range 11-20 km. The total wind variation is considered proportional to the thickness of the distinct layer over which it acts. The data show the mean value of the maximum shears to be 0.0088 sec^{-1} , and extreme values about 0.018 sec^{-1} .

The limitations of the present data, the facts that they are in a quasi-Eulerian coordinate system, that they represent single sites, and that they do not include temperature data of a comparable vertical resolution, make confirmation of the model tentative at present. Further study should be based on a more complete set of measurements. The apparent relative simplicity of the flows at these stable levels of the atmosphere, as contrasted to those at lower altitudes, suggests that eventually the detailed forecasting of shears and turbulence may often be practical.

SECTION I INTRODUCTION

The increasing number of space vehicle launch operations has promoted application of the FPS-16 radar to tracking of superpressure balloons in order to measure the detailed wind structure of the atmosphere. The first published analysis of the data obtained from this tool (Stinson, Weinstein, and Reiter, 1964) verified the existence of wind speed and direction oscillations of amplitudes (5-10 m/s, 5-20 degrees) and of vertical wavelengths (0.5-2.0 km) which could materially affect the success of a space vehicle launch. It was found that these oscillations persisted at approximately the same altitude for periods sometimes exceeding six hours. Three models of mesoscale flow were suggested to account for these characteristics.

In the present report 11 additional series of wind speed and direction profiles, each containing from eight to eleven ascents covering 8 to 12 hour periods, are investigated in some detail. The profiles, obtained off the coast of Southern California, near Point Mugu, display characteristics similar to the earlier ones measured over Cape Kennedy, Florida. The increased data sample provides a more reliable statistical summary of the magnitude and depth of the previously revealed detailed features.

The usable section of the profiles is presently confined to altitudes above approximately 11 km, corresponding to the subcritical Reynolds number regime of the balloon where self-induced balloon motions are small and wind speed details can be measured to an accuracy of 1 mps. Below this level, where the balloon operates in the supercritical Reynolds number regime, self-induced motion is significant enough to mask certain wind details that exist (see MacCready and Jex, 1964, Scoggins, 1964, and Murrow and Henry, 1965, for a discussion of self-induced balloon motion, and Scoggins, 1965, for a discussion of a solution to this problem through the utilization of balloons with roughened surfaces).

The three models of mesoscale flow are critically considered. It is found that a model depicting the atmosphere from 11-20 km as being made up of a stack of thin, stable, quasi-horizontal layers, each covering a large horizontal area and each containing air whose motion is controlled by a somewhat independent quasi-inertial oscillation, best accounts for the main features of the persistence, magnitude, and horizontal extent of the wind fluctuations.

As an outgrowth of this model a crude forecast scheme is developed to utilize single station wind soundings to predict, for perhaps tens of hours, the maximum shears which can be expected. Nineteen series (the eleven previously mentioned, plus eight more which became available later) are incorporated into the empirically derived forecast scheme.

SECTION II. GENERAL CHARACTERISTICS

Figure 1 shows a sample wind speed and direction series (12-13 December 1963)

The scatter of data points below approximately 11 km is due to random balloon motion and is not necessarily indicative of the detailed wind structure. Above approximately 11 km, in the subcritical Reynolds number regime of the balloon, random motion is eliminated and a high degree of confidence can be placed in the profile details. At these levels the most significant features of the wind profiles are wind speed and direction fluctuations which persist, often throughout the whole series, at approximately the same altitude.

In describing the nature and characteristics of these fluctuations we may adopt an approach taken by the perturbation theory. Positive and negative anomalies in wind speed and direction may be regarded as oscillations about a mean wind profile, $\bar{V} = \bar{V}(Z)$, which should remain constant -- or nearly constant -- throughout the period of observation. From data such as those shown in Fig. 2 the condition $\partial\bar{V}/\partial t = 0$ is closely approximated by computing \bar{V} from the relationship

$$\bar{V} = \frac{V_1 + V_2}{4} + \frac{V_2 + V_3}{4} = \frac{V_2 + \frac{V_1 + V_3}{2}}{2} \quad (1)$$

where V_1 and V_3 are wind speeds at two consecutive minima (maxima) and V_2 is the speed of the maximum (minimum) between. (Similar considerations would hold for wind directions.) The value of \bar{V} thus computed is characteristic of the level

$$\bar{Z} = \frac{Z_1 + Z_3}{2}$$

The wind values actually measured in the wind profiles, examples of which are shown in Figs. 1 and 2, thus are composed of

$$V = \bar{V} + V^* \quad (2)$$

where V^* are the perturbation wind speeds. Their characteristics are the main objective of this study.

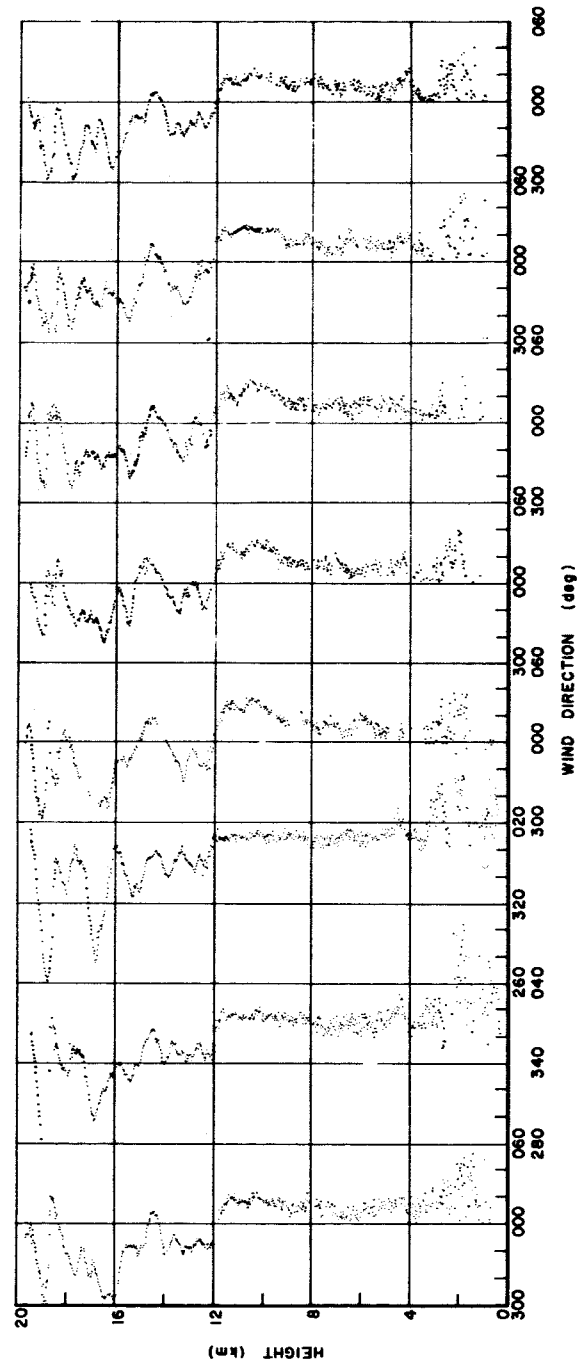
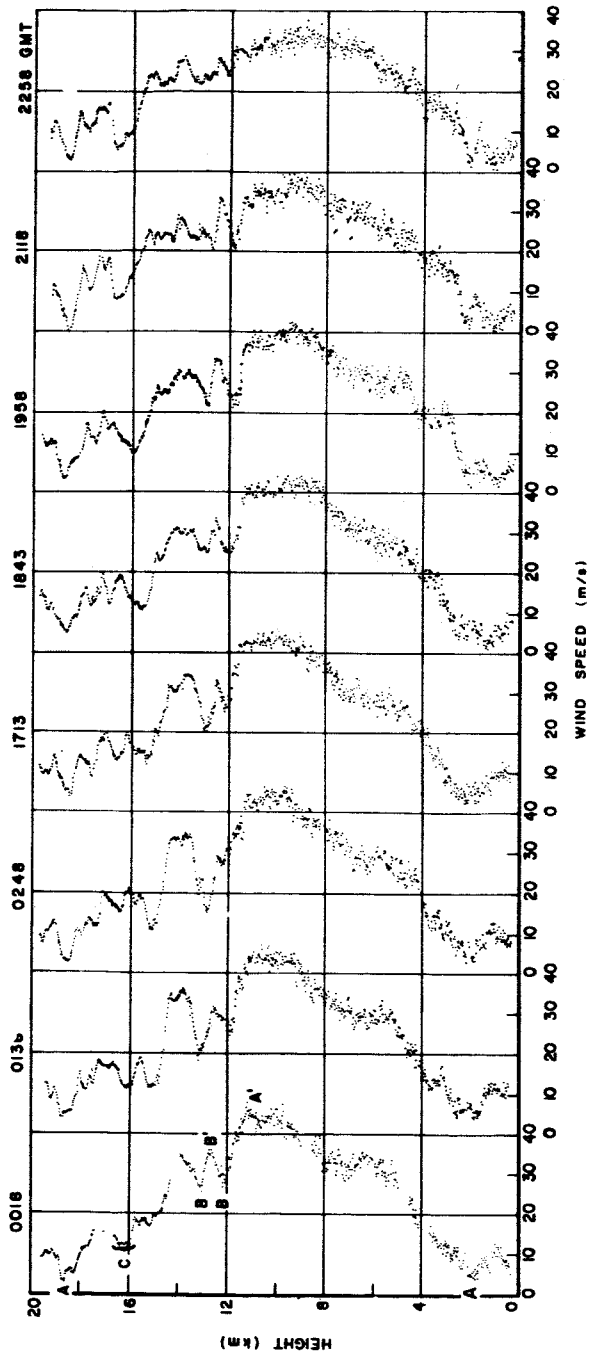


Fig. 1. SPEED AND DIRECTION PROFILES, 12-13 DECEMBER 1963

The amplitude of a particular perturbation in the wind profile may be defined as

$$A = V_2 - \bar{V} = \frac{V_2 - \left(\frac{V_1 + V_3}{2}\right)}{2} \quad (3)$$

where V_2 is the speed at a wind maximum (minimum) as defined earlier.

The vertical wavelength of the same perturbation is given as

$$L_Z = Z_3 - Z_1 \quad (4)$$

The normalized mean vertical wind shears above and below the level of a local extreme of perturbation speeds are

$$\frac{V_3 - V_2}{Z_3 - Z_2} \times 100 \quad \text{and} \quad \frac{V_2 - V_1}{Z_2 - Z_1} \times 100 \quad \text{respectively,} \quad (5)$$

in units of m/s per 100 m (or degree per 100 m if the same reasoning is applied to wind directions). In some cases the velocity shears are given in terms of sec^{-1} . The depths of the shearing layers are

$$(Z_3 - Z_2) \quad \text{and} \quad (Z_2 - Z_1) \quad (6)$$

In general they will differ from $L_Z/2$ if the perturbations are not symmetrical along the vertical coordinate, and/or if $\partial\bar{V}/\partial Z \neq 0$.

From Fig. 1 and from similar wind profiles it becomes evident that various scales of perturbations exist in the atmosphere. To each of these scales the considerations given in expressions (1) through (6) may be applied separately. Specifically, the following categories of wind speed perturbations may be recognized:

- (1) Large scale (jet stream) perturbations (A-A'-A in Profile 1, Fig. 1) having a vertical wavelength generally greater than 5 km, an amplitude greater than 20 m/s and usually persisting unchanged throughout the series.
- (2) Mesoscale perturbations (B-B'-B) having a vertical wavelength from 0.2 to 2 km and an amplitude from 1-15 m/s.

Individual wind speed maximums from these perturbations persist from several hours to a time period longer than that over which measurements were taken. Often the amplitude and occasionally the vertical wavelength of the perturbations change considerably from one profile to the next so that successive perturbations are usually not exact replicas of each other yet can still be identified as the same feature quite easily.

- (3) Small scale (turbulence) perturbations (several are found in region C) having a vertical wavelength less than 500 m and an amplitude less than 3 m/s. These oscillations differ from the small mesoscale ones principally because of their highly transient nature. They are common perturbations on a given profile but have no time continuity.

The mesoscale perturbations are of the major interest here. Figure 2 shows some of the common changes observed in these perturbations. Wind direction profiles display similar characteristics.

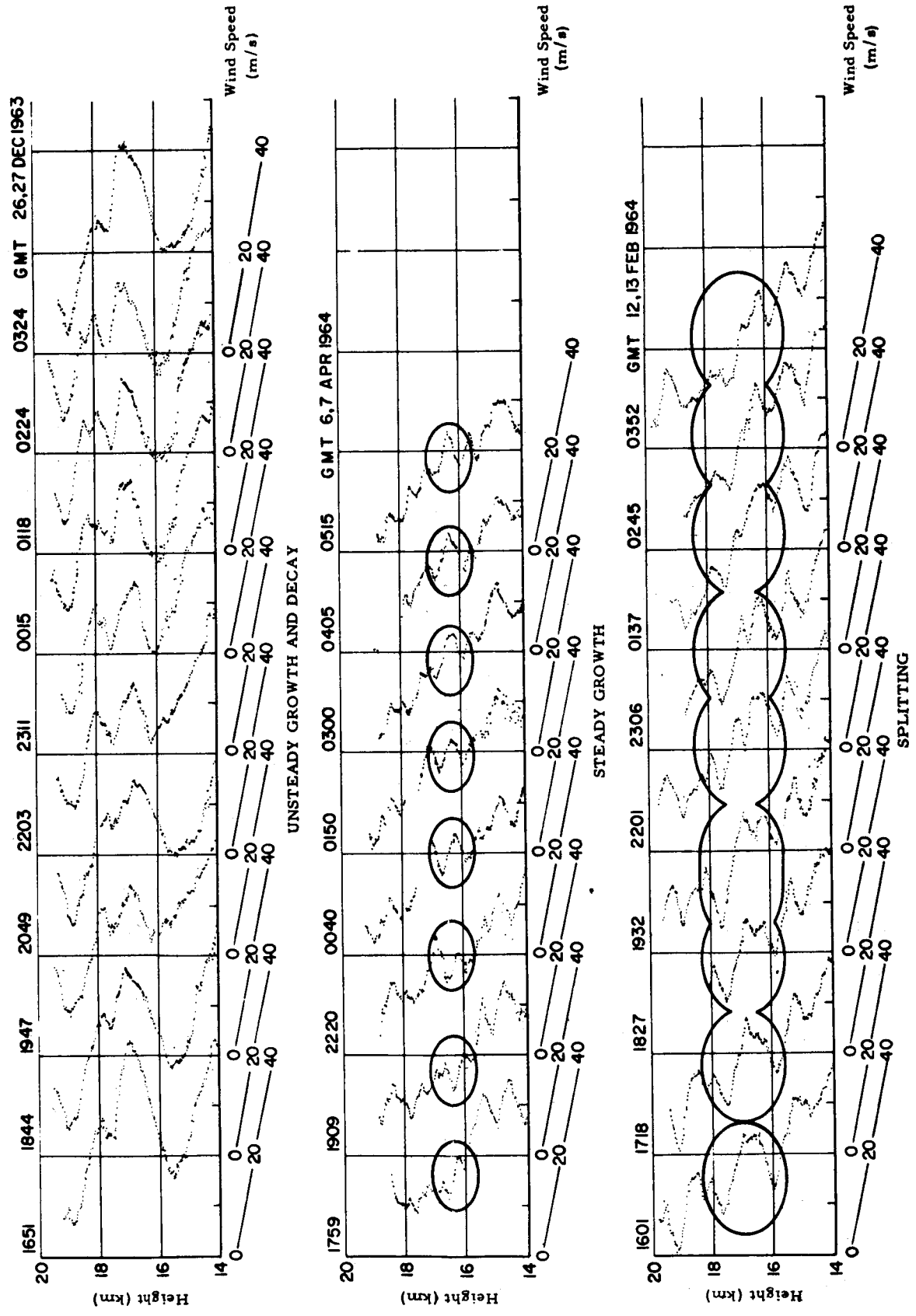


Fig. 2. COMMON CHANGES IN MESOSCALE PERTURBATIONS

SECTION III. DATA SUMMARY

A total of eleven series from Southern California, containing 98 individual wind speed and direction profiles from which approximately 4000 wind shears (2000 each of wind speed and wind direction) were measured, have been summarized. Appendix A contains a complete résumé of these data. It can be seen from the table that the small features, both turbulence and small mesoscale, were most prevalent in both the wind speed and direction profiles; however, more than 10 per cent of the normalized mean vertical wind shears exceeded 3.5 mps/100 m, 10 per cent of the winds turned more than 23 degrees/100 m, and 10 per cent of the depth of shearing layers exceeded 0.5 km. The latter figure indicates that over 10 per cent of the perturbations had vertical wavelengths exceeding 1.0 km.

The series of observations were divided into three types of synoptic conditions as determined by the 500-mb contour patterns: ridge (4 series), trough (2 series), and post trough (3 series). The last category included those observations taken within one day of the passage of a 500-mb trough. One series was not included in the synoptic study as it did not fit any of the synoptic categories. As may be seen from the table in Appendix A, there was no significant difference between the frequency of occurrence of the different wind features under the different synoptic conditions. As far as one may infer from the limited data sample, this result indicates that there is no dominating synoptic control over the profile fluctuations.

Two series from a previous study at Cape Kennedy, Florida, were analyzed in the same way. It was found, at least for the wind direction, that the small changes (0-4.99 deg/100 m) were considerably more frequent at the Florida site than in California (82 per cent versus 34 per cent). Due to the small data sample at Cape Kennedy, however, this result should be viewed with caution.

The table in Appendix B contains a complete listing of the joint empirical probability distribution of wind speed change and depth of the change layer. The principal aspect of this table has been qualitatively outlined in Fig. 3 by the isopleths of empirical probability. While the percentage of observations falling into any one class of wind speed change and depth of change layer is small, a definite trend toward increasing wind speed change with increasing layer depth is clearly evident.

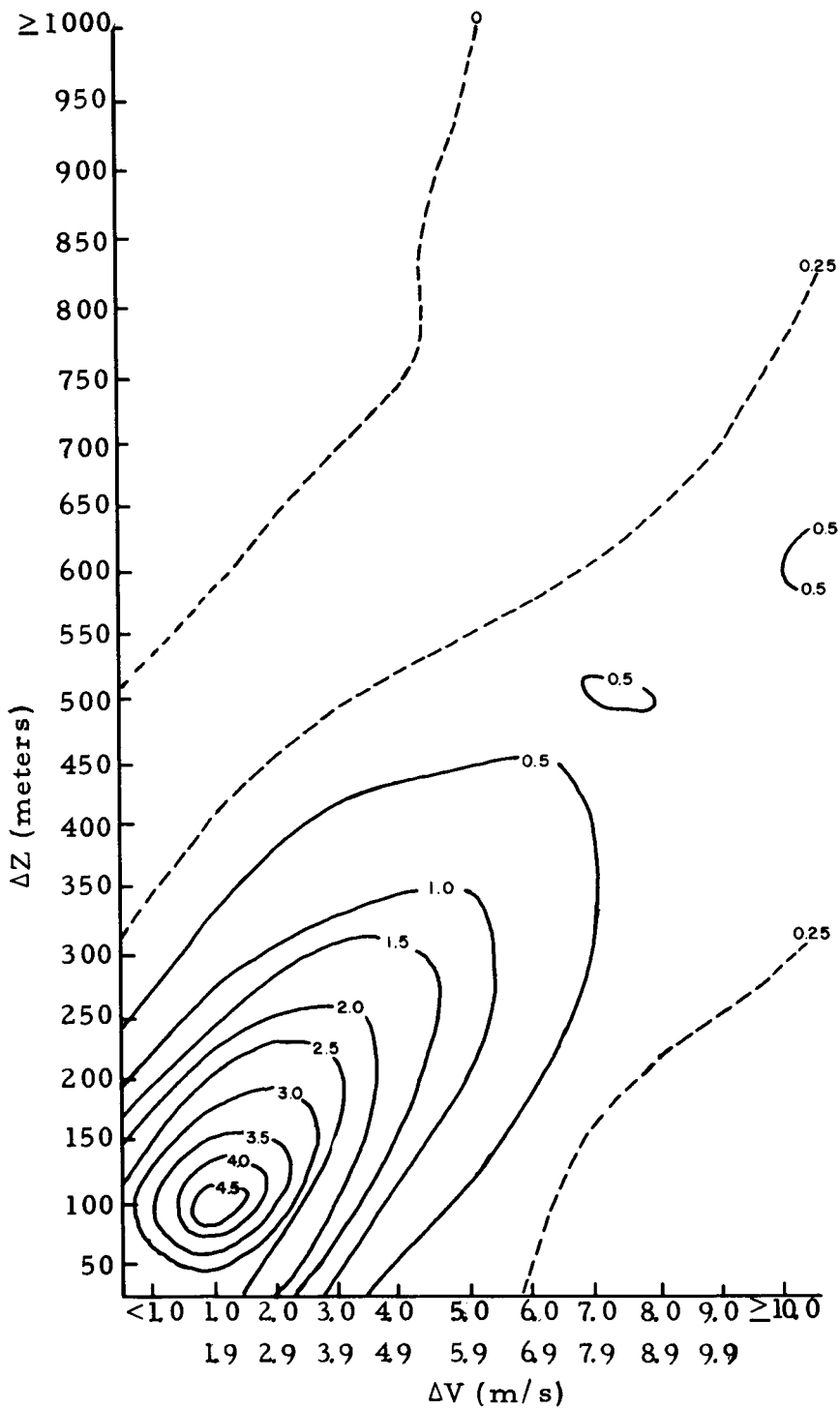


Fig. 3. SMOOTHED JOINT EMPIRICAL PROBABILITY DISTRIBUTION OF WIND SPEED CHANGE (ΔV) AND DEPTH OF THE LAYER (ΔZ) (Probability in per cent of total observations - 2088)

SECTION IV. MODELS OF MESOSCALE FLOW

Three models of mesoscale flow have been proposed to explain wind fluctuations similar to those observed in the present investigation.

A. Paired Longitudinal Vortices

The first model postulates stacked layers of oppositely directed or paired longitudinal vortices.

Avsec (1939) showed quite conclusively that, under controlled laboratory conditions, a large variety of paired vortices could exist. One of the principal features found by his study was that these vortices tend to undergo erratic fluctuations. At any given time a line of these, when viewed from above, displays a snake-like pattern.

Kuettner (1959) and Conover (1960) found evidence from cloud patterns showing that this type of flow exists in the atmosphere. Similar evidence was found from observations of soaring birds by Woodcock (1942), motion of tetroons by Pack (1962), ground dosages of tracers by Smith and Wolf (1963), and aircraft temperature and mixing ratio observations by Mee (1964). The general characteristics of the atmospheric vortices as indicated by these investigators are:

- (1) The ratio of horizontal to vertical dimensions are of the order of unity.
- (2) The lateral components of air motion are light (Conover found 0.6 to 6 m/s).

There have been no published accounts of stacked paired vortices. Brunt (1939) stated that vertical stacking of vortices is theoretically possible but would be a highly transitory phenomenon.

The tracks of the balloons used to calculate the wind profiles similar to those shown in Fig. 1 are plotted in Fig. 4. The inset in the lower left shows the separation rates of successive

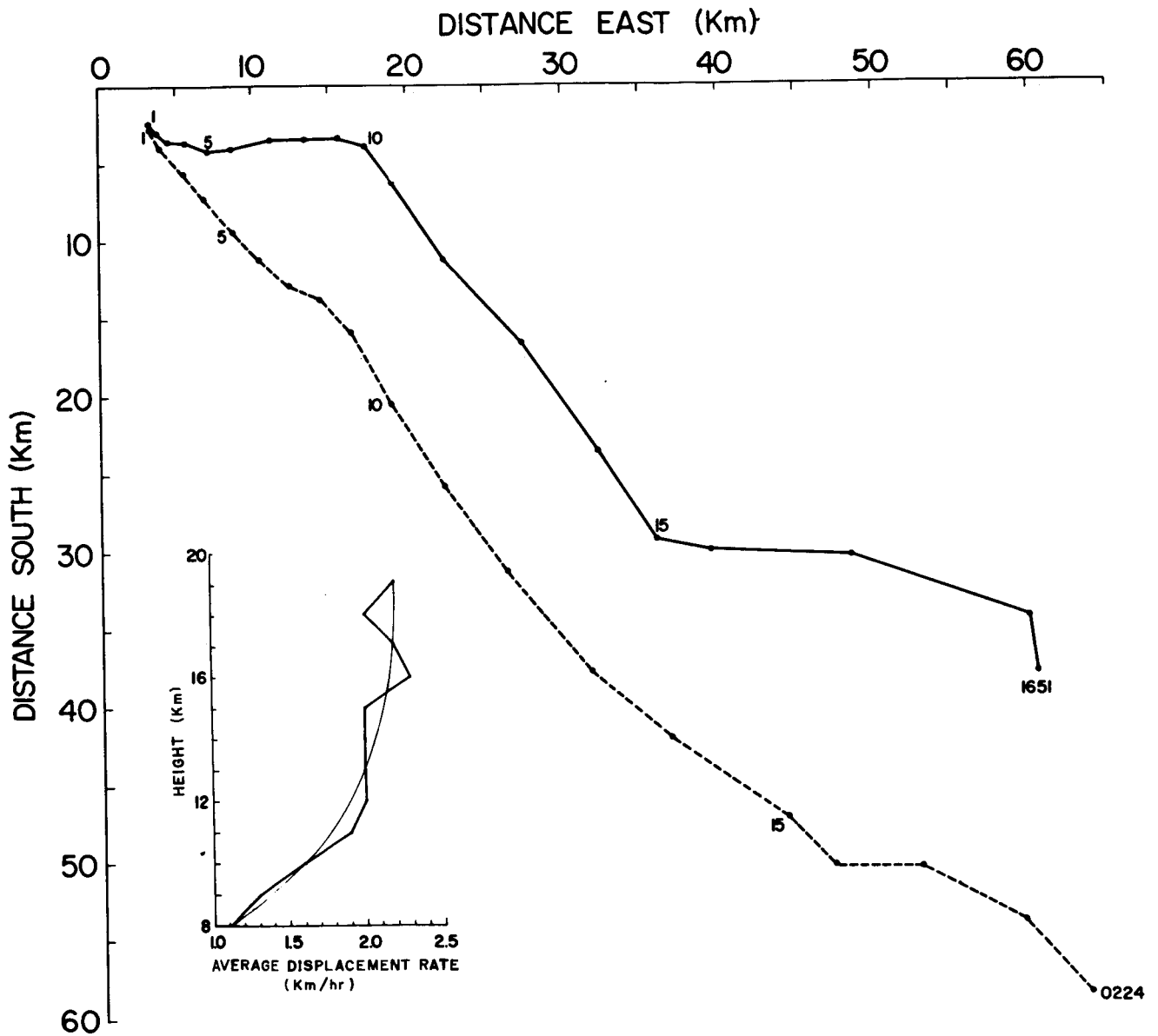


Fig. 4. SPHERICAL BALLOON TRACKS, 26-27 DECEMBER 1963

balloons. It can be seen that the same perturbation in the wind profiles (Fig. 5) was observed over a considerable horizontal area (approximately 20 km in the case of the perturbation at the 17 km level). The horizontal to vertical dimension ratio of paired vortices which could be responsible for such wind fluctuations would have to be an order of magnitude larger than their theoretical value derived by Avsec and anywhere from two to ten times larger than the maximum values observed by the other authors.

Another apparent problem with the longitudinal vortex theory relates to the three-dimensional vortex motion. The circulation must include substantial vertical air motions between the horizontal boundaries. This vertical motion, taking place adiabatically, would require a temperature sounding close to neutral within the vortex layer. The temperature profiles, although crude, have sufficient accuracy and vertical resolution to show that such near-neutral regions are not associated with the velocity oscillations in many cases.

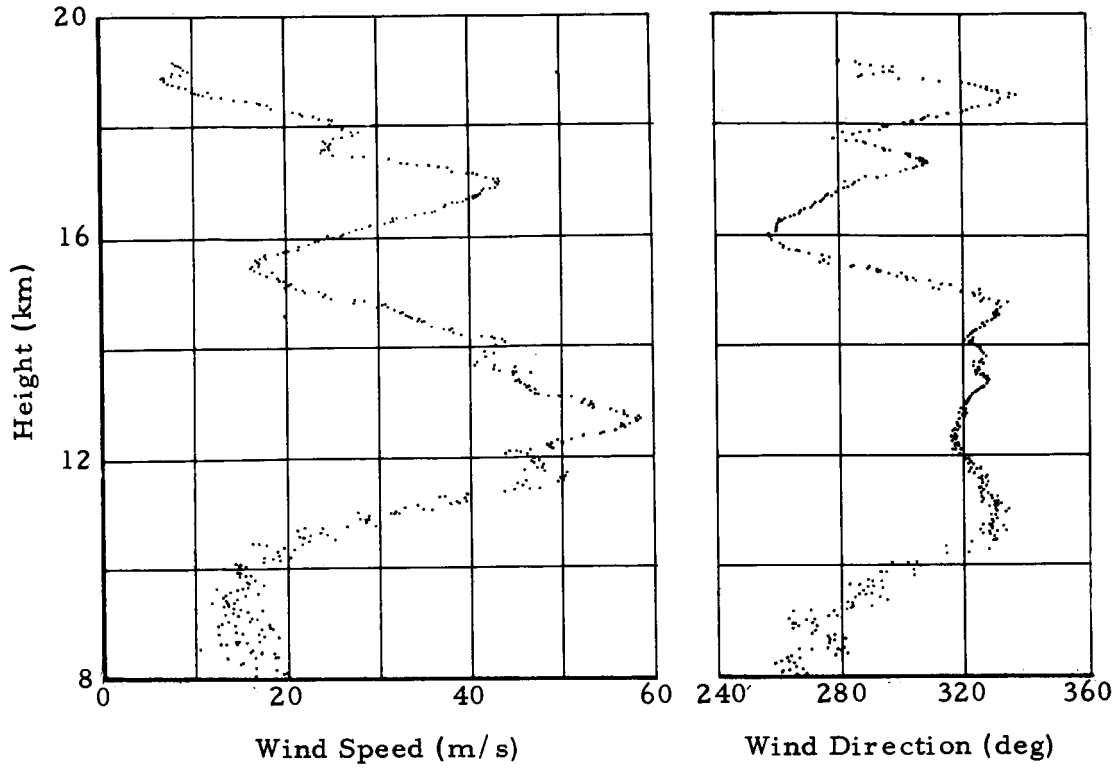
A further major drawback to this model is the observed persistence of the wind fluctuations. It is difficult to conceive of such shallow and hence narrow vortices remaining in an exact orientation relative to successive ascending balloons for many hours (particularly as successive balloons sometimes cover different geographic paths as shown in Fig. 4).

Since it has been clearly shown that paired longitudinal vortices exist in the atmosphere, they may be reflected in the small transient wind perturbations observed in the detailed wind profiles. They do not, however, appear to be the cause of the persistent mesoscale perturbations.

B. Internal Gravity Waves

The second model is frequently employed to explain perturbations in wind profiles similar to those observed in the present investigation. This model explains the perturbations as manifestations of internal gravity waves. The horizontal velocity variations are deemed to be the result of a thickening or thinning of the layer containing them, as the air moves through gravity waves

26 December 1963, 1651 GMT



27 December 1963, 0224 GMT

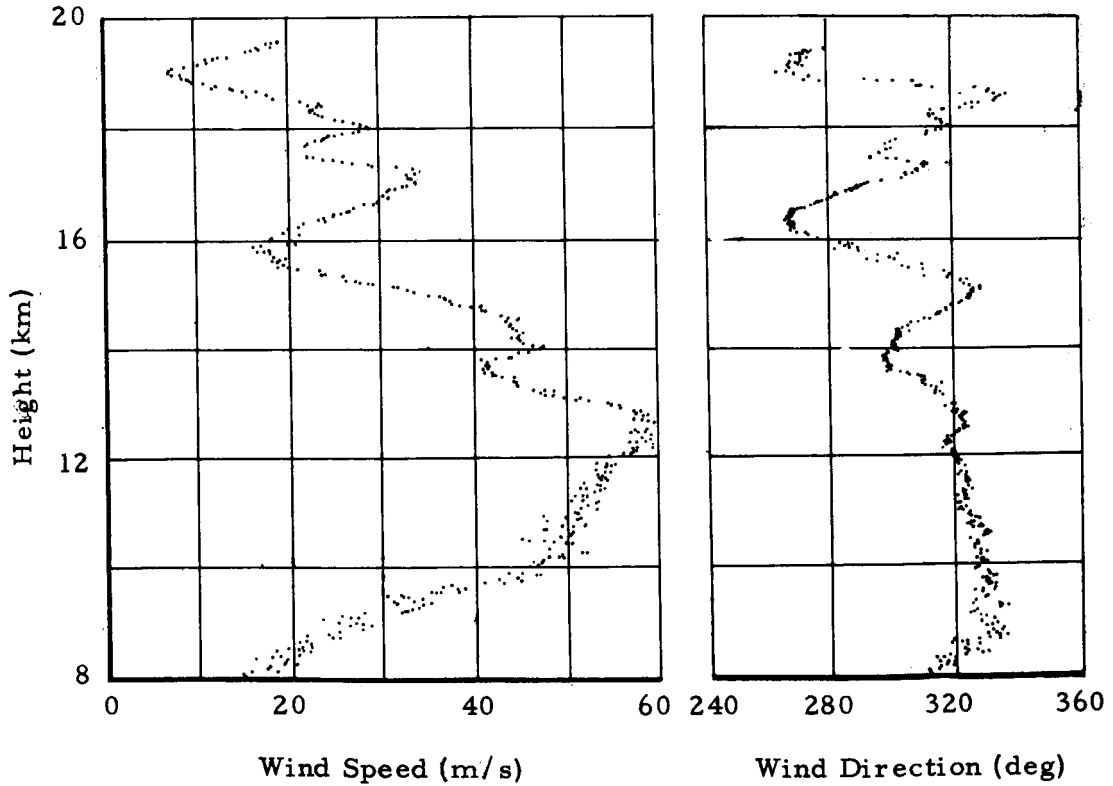


Fig. 5. SPEED AND DIRECTION PROFILES, 26-27 DECEMBER 1963

which are not in phase in the vertical. Hines (1960) gives a thorough description and theoretical treatment of this mechanism. He showed that it could be responsible for observed wind speed features in the stratosphere with vertical wavelengths of 12 km. When his equations are applied to vertical oscillations in the altitude range from 11-20 km, it is found that the vertical wavelengths of the wind oscillations with a period of 10 hours should be two orders of magnitude less than the horizontal wavelengths of the gravity waves. In the present context, standing gravity waves (lee waves) must be investigated first as a perturbation source as they offer the best explanation of the persistence of the wind fluctuations. It could be postulated that the standing waves are generated by the thermal and frictional differences between land and sea along the coasts of California (present data) and Florida (previous data). Lee wave theory, however, states that the horizontal and vertical wavelengths should be of the same order of magnitude. In order to make this statement consistent with the calculation mentioned above (i. e., to say that the wind features from 11-20 km altitude, where the horizontal wavelength exceeds the vertical by two orders of magnitude, are manifestations of standing gravity waves near the surface of the earth where lee wave theory states the wavelengths should be the same order of magnitude), it must be postulated that the horizontal wavelengths increase by 200 times within less than 20 km height. At the present there is no indication of such a wavelength increase.

In an effort to determine the order of magnitude of the horizontal wavelength of a lee wave which could be produced with the wind speed and temperature profiles observed on 26 December 1963, the l^2 profile, as defined by Equation (7), was drawn.

$$l^2 = \frac{g}{\theta} \frac{\partial \theta}{\partial Z} / v^2 \quad (7)$$

Lee wave theory calls for the maximum horizontal wavelength to be found at the level of minimum l^2 and for the wavelength to be given by Equation (8).

$$\lambda_{\max} = \frac{2\pi}{l_{\min}} \quad (8)$$

The minimum ρ^2 was 0.02 and the resulting maximum horizontal wavelength was 45 km. Hines' theory calls for a gravity wave with a horizontal wavelength of approximately three times this value to produce the perturbation observed in the vertical profile on 26 December at 17 km.

While these numerical values fall into the right order of magnitude, they have been obtained by extending the lee wave theory considerably beyond its original applications.

Free internal gravity waves may be a source of wind fluctuations such as the observed ones only if the ratio of horizontal to vertical wavelengths is of the order of 100:1. In this case they propagate very slowly and behave almost like a stationary phenomenon. These waves, however, would produce wind speed perturbations an order of magnitude smaller than those observed in the present data. In order to produce wind speed perturbations of the observed order of magnitude, a period of approximately one to two hours is required. This does not conform to the persistence of perturbations over at least six hours, evident from the data presented here.

C. Quasi-Inertial Oscillations

The third model under consideration calls for stacked layers of air undergoing quasi-inertial oscillations. These layers are relatively thin and stable and -- unless turbulent forces or convective motions are present -- could maintain themselves for considerable periods of time and over wide areas.

Danielsen (1959, 1964) directly, Kroening and Ney (1962) from ozone concentration measurements and Bigg (1964) from twilight scattering of particulate matter showed the existence of the laminated thermal structure of the atmosphere in agreement with the thin stable layers of the model. This structure could be expected to persist well beyond the 10-12 hour periods covered by the serial ascents.

Application of inertial oscillations to atmospheric flow phenomenon can be found in papers by Raethjen (1958) and Newton (1959) on axial velocity streaks in the jet stream, by Blackadar (1957) on the low level jet in the boundary layer and by Sawyer

(1961) on wind profiles over Crawley, England, very similar to those of the present investigation. These papers show that inertial oscillations may be more common in the atmosphere than traditionally believed.

The word quasi is inserted because the geostrophic basic flow about which oscillations occur may not necessarily remain constant in time. Furthermore, frictional forces and diabatic effects may have modifying influences. Even if the complicating factors were not present, a true inertial period of half a pendulum day (about 22 hours at the geographical latitude of the wind observations) need not be observed in the single station series of balloon ascents, as inertial motions of air parcels are described in a Lagrangian coordinate system. Their behavior in an Eulerian system, in which the present data are described, depends upon the advective properties of the oscillations, about which only assumptions can be made.

In spite of the limitations mentioned above, this model could easily account for the two characteristics of the observations, the persistence and horizontal extent of the perturbations. While this mechanism is probably not the only one operating on the wind fluctuations, it appears to be the most important one.

In evaluating the plausibility of the explanation of the shears as manifestations of inertial oscillations, one should consider whether geostrophic wind variations in the vertical could be strong enough to account for the observed shears. Taking an extreme horizontal temperature gradient such as associated with jet stream conditions, say, $5^{\circ}\text{C}/100\text{ km}$, yields a vertical gradient of geostrophic wind speed of about 0.02 sec^{-1} , several times stronger than the shears found here. However, the shears of this study often alternate in sign, and if generated solely by geostrophic wind would require unreasonable vertical temperature gradients (some of the gradients being self-destroying because of instability). The dominant wind oscillations for the normal weather situations studied here must be ageostrophic.

SECTION V. EFFECTS OF QUASI-INERTIAL OSCILLATIONS ON WIND PROFILES

In this section it will be shown how quasi-inertial oscillations could produce a persistent mesostructure in the wind speed and direction profiles and some of the characteristics these profiles would possess.

Consider the wind at a particular level (V_T) to be made up of a geostrophic component (V_g) and an inertial component (V_i) (Fig. 6). The former is constant in both magnitude and direction, while the latter is constant in magnitude but rotates anticyclonically with the period of the quasi-inertial oscillation. It can be seen that total wind at any instant depends upon the phase of the inertial cycle at that time.

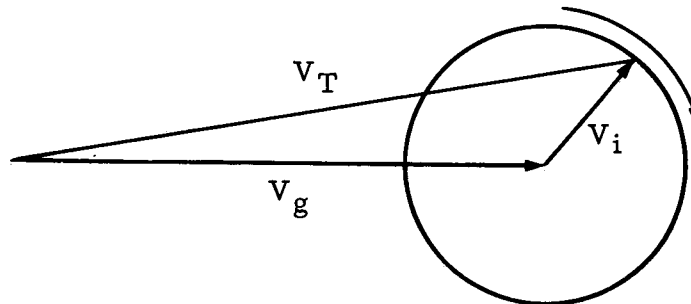


Fig. 6. VELOCITY VARIATION THROUGH AN INERTIAL CYCLE

Let us envision several such inertial circles stacked vertically and superimposed upon a profile of basic geostrophic flow which -- for simplicity's sake -- is assumed to have constant vertical shear above and below the level of maximum wind. In Fig. 7 independent inertial oscillations, similar to Fig. 6, are assumed at levels 1-7. The geostrophic component of the wind is shown by the dashed arrows, the total wind by the solid arrows. If each layer of inertial motions were completely detached from its surroundings, vertical discontinuities in wind speed and direction would result. These, of course, could not be maintained under the influence of turbulent forces. Such forces would tend to generate finite shears between layers. In the schematic profiles

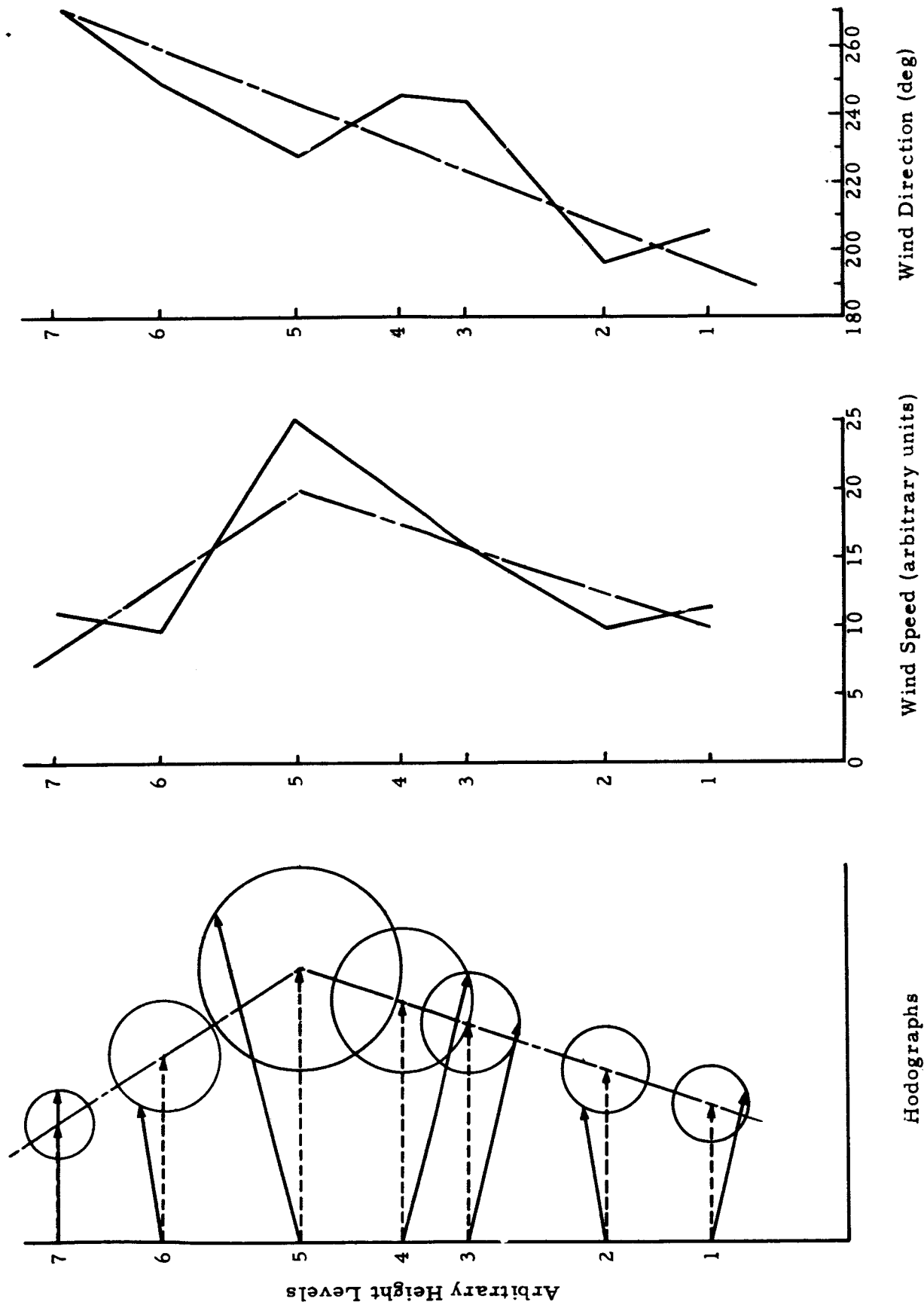


Fig. 7. ILLUSTRATIVE MODEL OF STACKED QUASI-INERTIAL OSCILLATIONS

of wind speed and direction of Fig. 7, linear shears were assumed to extend between the centers of each oscillating layer in line with observational evidence (Fig. 1). A vertically rising balloon, encountering oscillations at a different phase, thus would measure the wind profiles shown in the righthand portion of Fig. 7.

The following characteristics of wind speed and direction profiles should be noted:

- (1) No definite phase relationship between wind speed and direction perturbations is expected if the phase angles at which individual inertial oscillations are encountered remain undetermined.
- (2) For a true inertial oscillation, a maximum (minimum) deviation from geostrophic wind speed should correspond to a minimum (maximum) deviation from geostrophic wind direction.
- (3) The maximum vertical wind shears occur where two successive inertial oscillations are directly out of phase and the ageostrophic wind shear thus generated has the same signs as the basic geostrophic shear. The total wind direction change with height in such a situation is simply given by the geostrophic wind direction profile.
- (4) Maximum changes of wind direction with height should be found when two successive inertial oscillations are directly out of phase, one-quarter of a cycle removed from the time of maximum wind shear. The vertical wind shear in this case is given by the geostrophic wind speed profile.

SECTION VI. EVIDENCE IN SUPPORT OF THE QUASI-INERTIAL OSCILLATION MODEL

A. Temperature Soundings and Richardson Number

The existence of the horizontal inertial oscillations depends on the suppression of momentum exchange by turbulent mixing in the layers in question. Thus the temperature soundings should show stability at appropriate layers. Actually stability must be interpreted by Richardson Number, Ri , rather than from temperature profiles alone. The critical value of Ri differentiating between decaying and growing turbulence has not yet been accurately defined; values of 0.5 to 1.0 are in common use. Thus $Ri < 0.5$ denotes turbulence, $Ri > 1.0$ means stability, and $0.5 < Ri < 1.0$ is indeterminate.

The only temperature data available for the period of the FPS-16 wind soundings stem from standard radiosonde runs and have much less vertical resolution than the corresponding wind data. On Fig. 8 the temperature sounding is given together with the associated wind speed and direction profiles. The layers of temperature inversion are shown. There is no obvious correlation between these layers and significant points on the wind profiles.

Figure 8 also shows the profiles of Ri ¹. Here the correlation between details of stability and velocity is somewhat easier to interpret. There are three layers (at 12, 14, and 18 km) where Ri is very large, and each one can be associated with a shallow region of a double reversal of wind speed. The large single velocity peaks at 13 and 15.5 km are in regions of low Ri between layers of high Ri . Some turbulence evenly distributed through a layer undergoing an inertial oscillation should cause the velocity peak in the center of the layer.

The exact description and interpretation of the profiles of wind, temperature, Ri , and turbulence, and of their development

¹The use of Ri computed from a single wind and temperature profile is valid in this case as it has been shown that the features are very consistent. Ri was computed over layers within which both temperature lapse rate and wind shear were linear, the depth of the layers ranged from 100 to 1000 meters.

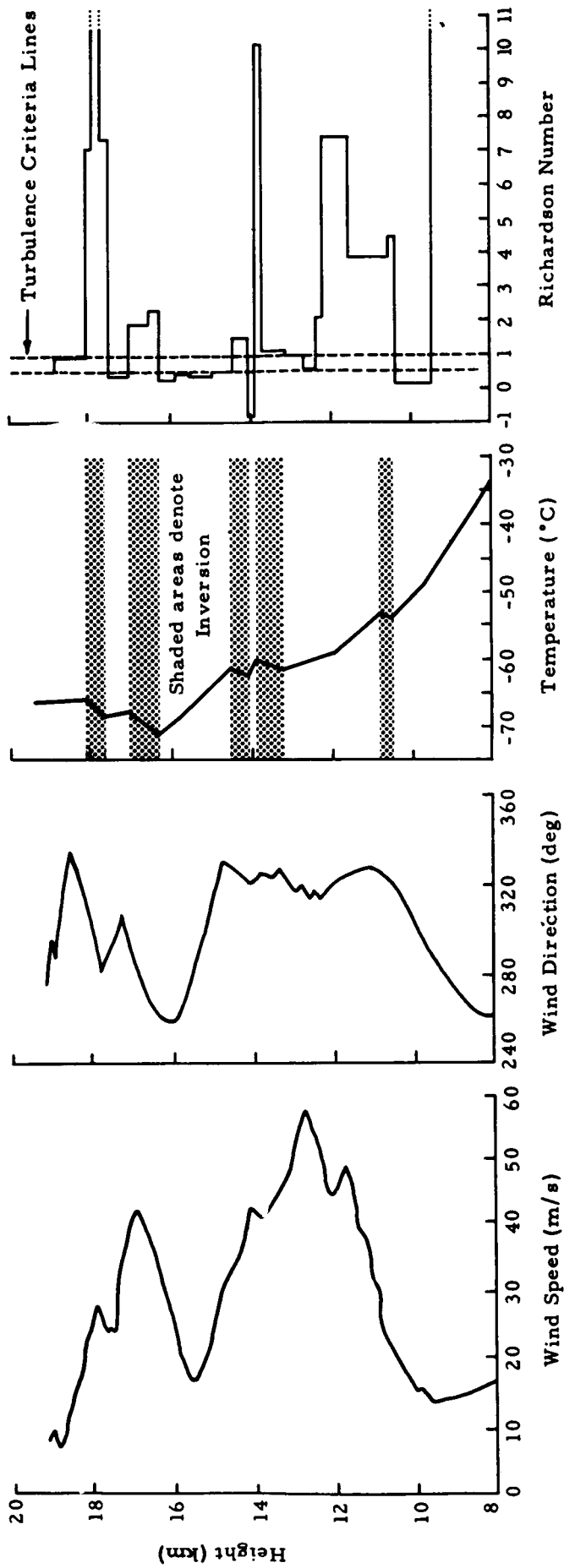


Fig. 8. SPEED, DIRECTION, TEMPERATURE, AND Ri PROFILES (1651Z, 26 December 1963, Western Test Range, California)

from previous profiles, must await the obtaining of more suitable measurements. The first crude interpretation given above, based on Fig. 8, provides encouragement that the physical principles related to Ri will prove to be valid in this application.

B. Wind Profiles

The present data measure perturbations in a quasi-Eulerian system ("quasi" because successive balloon soundings do not measure winds in precisely the same location). While this is of no serious consequence in macroscale observations and analyses, it may have some bearing on meso- or microscale considerations. Inertial oscillations, however, are defined in the Lagrangian coordinate system. From single-station analysis, therefore, the presence of such oscillations can only be inferred.

Another difficulty presents itself in the necessity of removing the "basic" field of flow (the geostrophic wind profile) from the measurements in order to arrive at the perturbations. This process still involves a certain amount of subjectivity. The subjectivity can be partially resolved by employing objective computational techniques. However, the data from a single sounding can never give enough information to permit the calculation of geostrophic wind to the accuracy really desired. Eventually more accuracy is of course obtainable by including other wind soundings, differing in time and location, and by using three-dimensional temperature field data.

Figure 9 shows, as an example, the wind speed and direction profile of 28 January 1964, 2139Z. With what has been said in describing Fig. 7, no phase relationship between peaks in either profile should be expected in an individual sounding, as the phase at which the balloon intercepts the successive oscillations remains undetermined.

If one inspected an individual perturbation in successive soundings, one should find changes in the speed and direction of the perturbation component according to the changing phase of the inertial cycle (see Fig. 7). It turns out, however, that such systematic changes are difficult to detect, because minor adjustments in "the basic flow profile" to be subtracted from the measured

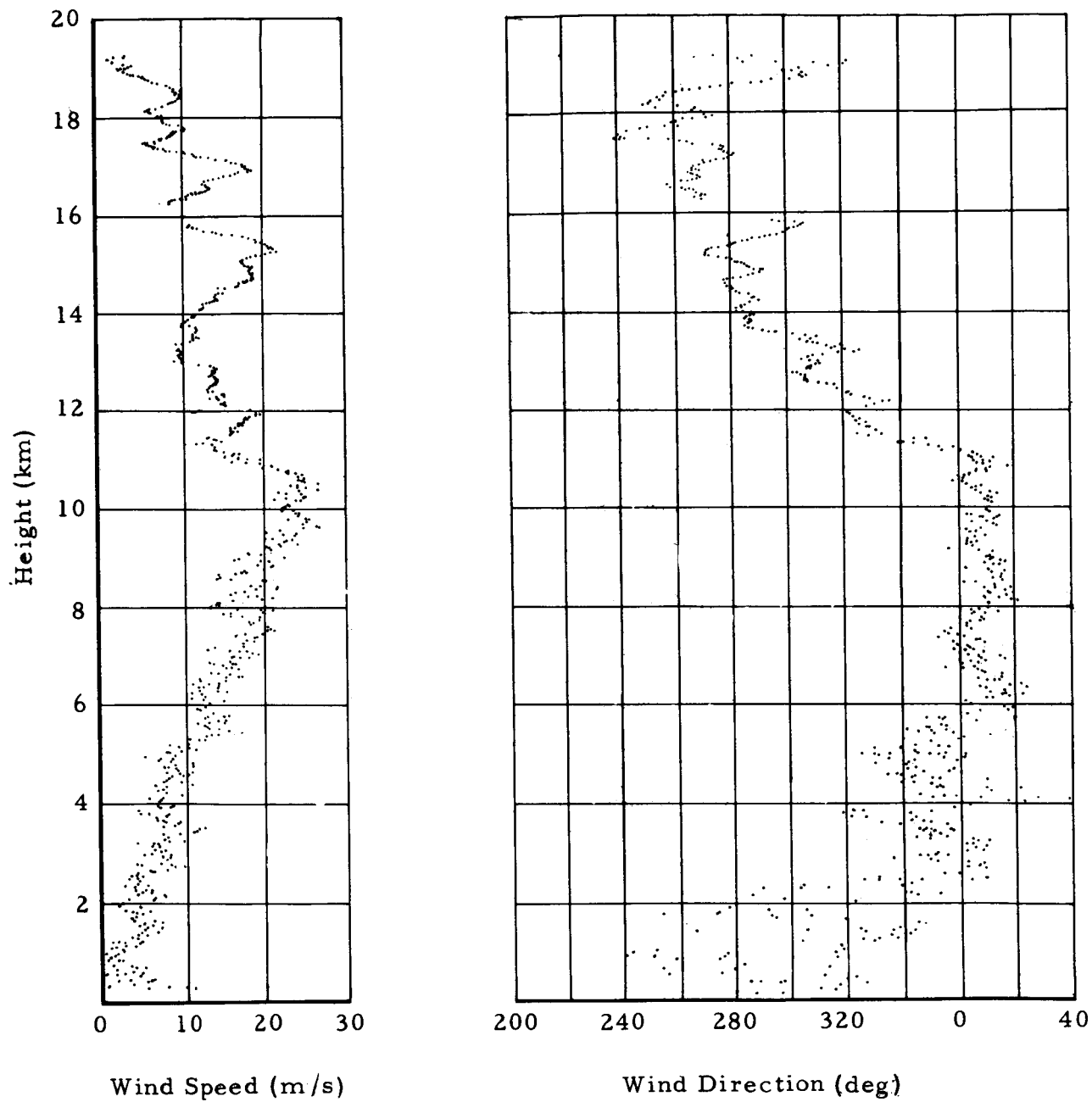


Fig. 9. WIND SPEED AND DIRECTION PROFILES, 2139Z,
28 JANUARY 1964

winds may alter the phase relationship between speed and direction fluctuations quite significantly. No statistical evaluation of such relationships, therefore, has been presented. Qualitative evidence in support of such a phase relationship, however, has been observed in the data.

SECTION VII. POTENTIAL CAUSES OF QUASI-INERTIAL OSCILLATIONS

Raethjen (1958) has pointed out that subgeostrophic components of flow may be introduced into the tropopause region by large convective systems. These systems would transport air masses with relatively small horizontal momentum upwards into an environment with high wind speeds. Such a process could conceivably trigger inertial oscillations downstream from the convective source region.

Mountain ranges also may serve as sources of ageostrophic components: on a large scale, by generating low pressure systems in the upper flow pattern on their lee side, and on a smaller scale by producing mountain waves under suitable atmospheric conditions.

A large number of persistent perturbations in the FPS-16 wind profiles are observed above tropopause level in a thermally stable environment. Convective processes in the troposphere may have to be ruled out, therefore, as a potential source for these perturbations. Mountain effects, however, are known to reach to even higher levels in the stratosphere.

Jet stream systems with their associated accelerations and decelerations contain ageostrophic components of flow in deep layers. The thermal structure of the atmosphere also shows a great amount of detail in their vicinity (Danielsen, 1959; Reiter, 1963; Reiter and Mahlman, 1964).

The wavelengths of quasi-inertial oscillations is a function of the "basic flow", \bar{v}

$$L = a \frac{2\pi}{f} \bar{v} \quad (9)$$

(the factor a is equal to 1 for true inertial oscillations, larger than 1 for oscillations in which the geostrophic field of flow adjusts itself slowly to the perturbations (Newton, 1959)). If in a region of geostrophic vertical wind shear,

$$\frac{\partial v_g}{\partial z} \neq 0$$

an ageostrophic component of motion is introduced in a deep layer with the same sign and similar magnitude (as might be the case in the vicinity of a jet stream system), the dispersive characteristics of Equation (9) would cause a phase shift of inertial oscillations in successive vertical layers of the shearing flow downstream from the source region of the ageostrophic component.

We might now postulate that a certain thermal structure, consisting of a succession of more and less stable layers, is originally present in the atmosphere where the inertial oscillations are generated. The vertical wind shears produced by the dispersive properties of Equation (9) would lead to exchange processes in the less stable regions, while the more stable layers would contain the quasi-inertial oscillations at nearly full magnitude. Wind profiles similar to the ones observed may thus result.

Unfortunately, at this time no details are known about the full extent in space and about possible phase changes of the wind perturbations observed by FPS-16 radar. The above reasonings, therefore, have to remain purely speculative and should be considered only as suggestive for further research.

SECTION VIII. FORECASTING APPLICATION

One of the principal aims of the present investigation is to provide space vehicle operations with an estimate of extreme wind conditions to be expected during the launch period. The concepts outlined in the previous sections, combined with empirical data from nineteen sets of serial ascents, have been incorporated into a forecast nomograph capable of indicating the extreme wind shears that might evolve from a given wind speed profile.

The idealized combination of stacked quasi-inertial oscillations shown in Fig. 7 illustrated the conditions leading to extreme shears. Such conditions of a pair of directly out-of-phase quasi-inertial oscillations occurring in adjacent layers are rather unlikely. It is more likely, however, for successive oscillations to be at least slightly out of phase. In a given period of time the phase relationship between successive layers will change, as may be inferred from Equation (9). At some time such changes will bring about certain periods in time, as well as areas in space, in which -- under the given conditions of atmospheric stratification -- vertical shears associated with any one pair of inertial oscillations will reach relatively large values. Their absolute maximum should be attained whenever two adjacent inertial oscillations are superimposed 180° out of phase. During a series of balloon ascents this ideal case may never occur. "Maximum" shears evaluated from such series, therefore, may not be quite as large as these possible absolute maxima.

If, on a large number of serial ascent sets, one follows individual perturbations and notes their vertical wavelengths (λ_z) and maximum amplitudes (ΔV_{\max}), one obtains a statistical measure of the maximum shears. This was done with the nineteen sets of serial ascents from California. There were 132 well developed oscillations incorporated into the statistical analysis.

Figure 10 shows plots of λ_z versus ΔV_{\max} for high (maximum wind speed in the jet cone > 35 m/s) and low wind speed cases. It can be seen that the scatter of points is small and that the data for the two cases tend to diverge when the vertical wavelength gets above 2.0 km. As the oscillations in question rarely attain such large vertical wavelengths, it was decided to recombine all of the data into one nomograph (Fig. 11). Here the axes are labeled in terms of speed change and depth

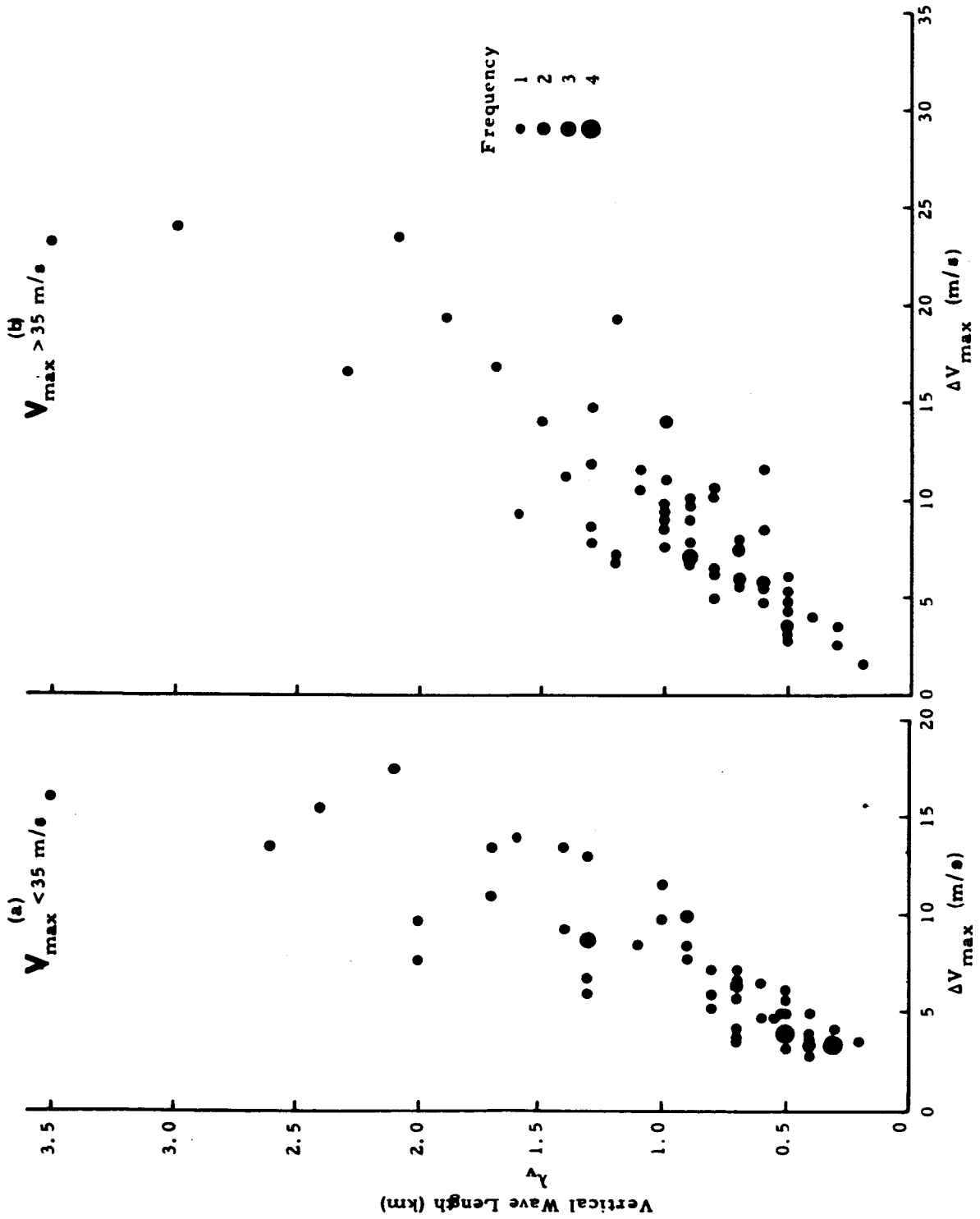


Fig. 10. PLOT OF AMPLITUDE (ΔV_{\max}) VS. VERTICAL WAVELENGTH (λ_v) FOR VERTICAL OSCILLATIONS AT THE MAXIMUM DEVELOPMENT

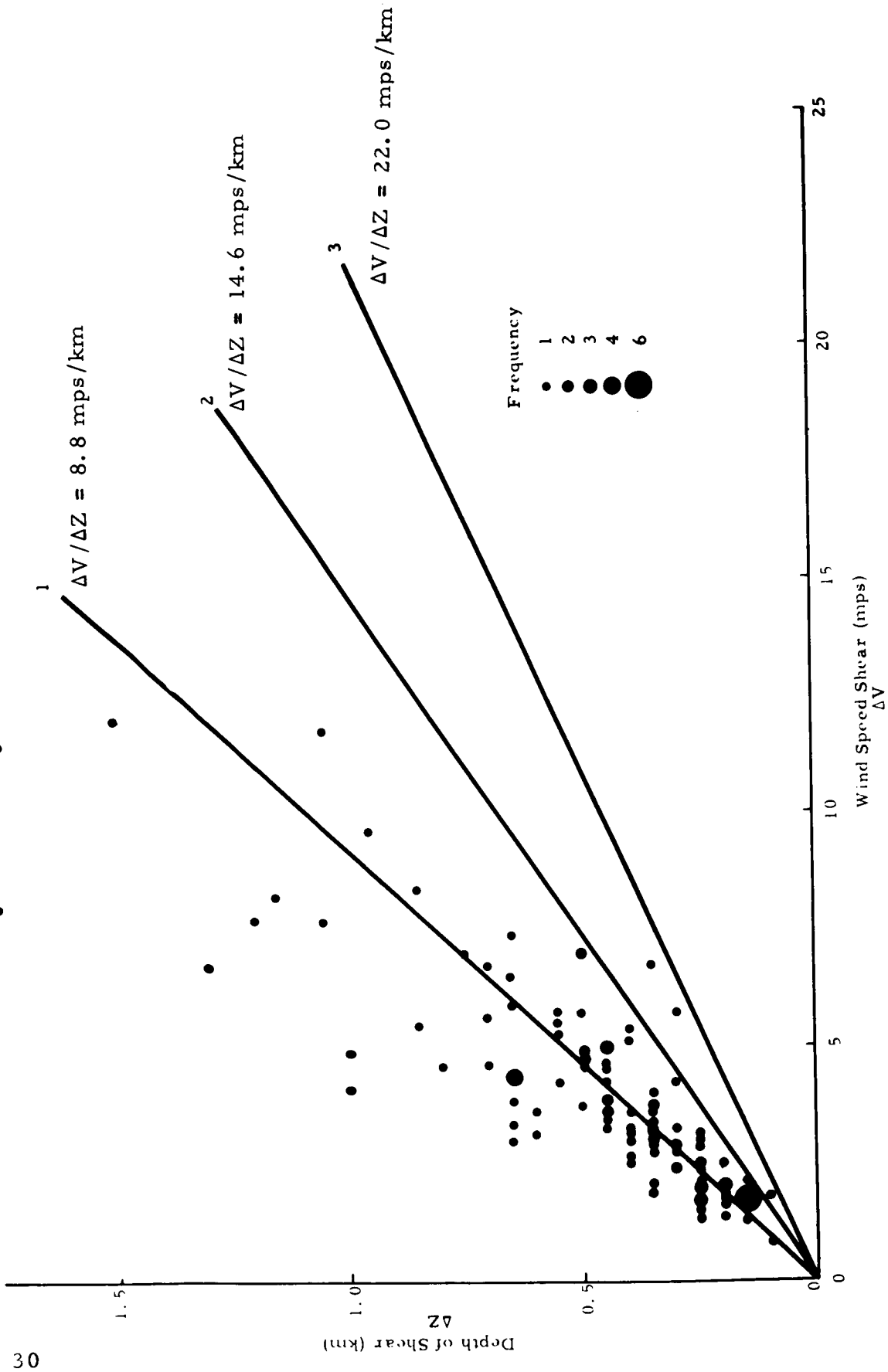


Fig. 11. FORECAST NOMOGRAM

of the change layers rather than amplitudes and vertical wavelengths. The straight lines labeled 1, 2, and 3, respectively, depict mean of all the data points, the 97.5 per cent probability (i. e. 97.5 per cent probability that future shears will fall to the left of this line), and the limiting shears by Richardson's Criterion assuming $Ri = 1$,

$$\frac{\partial T}{\partial Z} = 0 \quad \text{and} \quad T = -73^\circ\text{C}.$$

The lines labeled 1 and 2 in Fig. 11 were derived from the frequency distribution of maximum shears shown in Fig. 12, where the solid curve shows the fitted normal distribution, the dotted lines highlight the mean and the 97.5 per cent probability shears, and the dashed curve indicate limiting shears by Richardson's Criterion (assuming $Ri = 1$ at critical) for the indicated temperature lapse rates.

Figures 11 and 12 show that, from the data analyzed, the maximum vertical shears for any distinct layer practically never exceed 18 mps/km (0.018 sec^{-1}). This limit, or any other particular value as shown on the figures, can be used in a simple forecast scheme for maximum shears:

- (1) Several hours previous to launch time an FPS-16 wind profile is obtained.
- (2) The depth of the shearing layers of each oscillation are measured.
- (3) A synthetic wind speed profile is constructed using the above depths and the shear limit of, say 0.018 sec^{-1} . This synthetic profile may be assumed valid for as long as the thermal structure of the atmosphere (and consequently the depth of the shearing layers) remain the same. From the present data this seems to be the case for at least from 6-10 hours if no major changes in the upper flow pattern occur.
- (4) The synthetic profile is now compared with the originally measured one. If there is little difference between the two, it may be concluded that the oscillations were close to their maximum amplitude and, if anything, might be expected to decrease. If, on the other hand, the two profiles looked appreciably different, intensification of the existing individual shears might be expected.

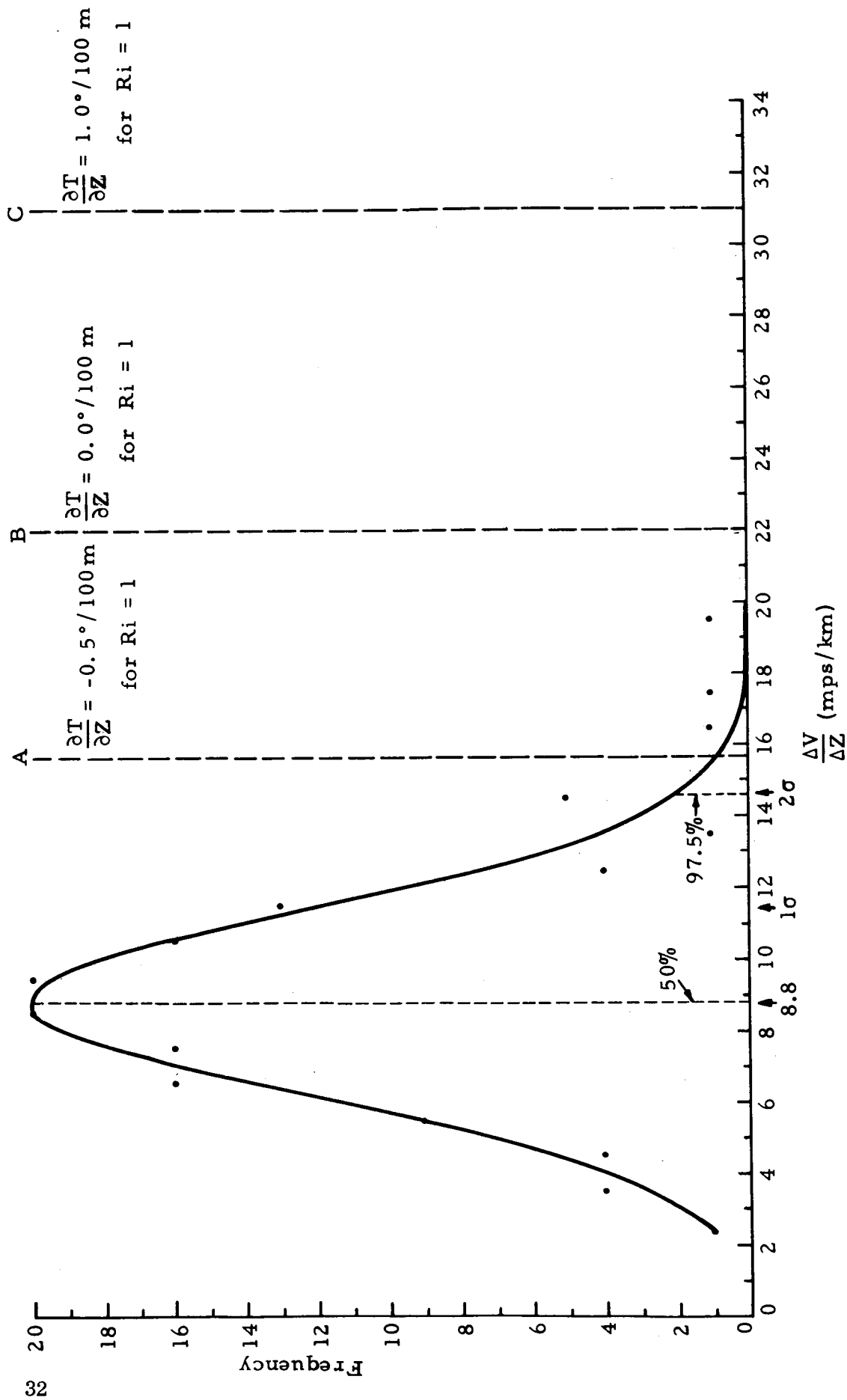


Fig. 12 FREQUENCY DISTRIBUTION OF SHEAR STRENGTHS

Whenever observed shears fall close to, or beyond, the line labeled 3 (limiting shears by Richardson's Criterion), turbulence should be expected in this layer and, as a consequence, the perturbation should break down. The points beyond or close to this line in Fig. 11 actually characterize perturbations which were observed to undergo considerable splitting in the course of time, similar to the one shown in Fig. 2 (Section II). It may be assumed that perturbations rendering data points far to the right of the mean line, and consequently near the line for $Ri = 1$, might break down, unless the local stability is much stronger than indicated by an isothermal lapse rate.

In this discussion, $Ri = 1$ has been used as a convenient reference without mention of the thickness of the layer in which Ri should be computed. In practice the thickness of this layer will be limited on the low end by the resolution of the temperature and wind data and on the high end by the depth of the shearing layers and/or inversion layers. For the present, a minimum layer depth of 100 meters appears most reasonable.

So far, only wind speed fluctuations have been considered, because they will yield a true perturbation component whenever maximum shears are produced by out-of-phase superposition of the quasi-inertial oscillations. Fluctuations of wind direction in vertical profile present a more complex problem. They should be evaluated in terms of perturbation vectors rather than in degrees of backing or veering of wind with height. The reason for this can easily be seen: a 10° change in wind direction over a layer of certain depth would produce quite different vector shears, thus different responses of the space vehicle when associated with 10 or with 30 m/s of total flow (i. e., $\bar{V} + V^*$), thus the shape of the geostrophic basic wind profile, as well as of the superimposed speed perturbations, will have to be considered when evaluating the possible effects of wind direction fluctuations on a vertically rising vehicle.

From Fig. 1 one may see that also wind direction perturbations show a marked tendency for persistence, thus one may eventually be able to forecast them. In view of the complex nature of their effect, however, no such attempts have been made yet.

SECTION IX. CONCLUSIONS AND RECOMMENDATIONS FOR FUTURE RESEARCH

Critical evaluation of the FPS-16 wind data made available so far suggests that the atmosphere from 11-20 km has a very layered mesostructure. The layers appear to be quite thin, stable, and have a large horizontal dimension. The data are quite consistent with the simple physical picture which says that, at altitudes where the air is generally stable (say 10-70 km), momentum exchange by turbulence is minimized and so thin horizontal layers will move horizontally relative to each other. Inertial oscillations about the geostrophic wind in each layer are very persistent and so, no matter what their cause, will tend to have random phases at any one time. Vertical shears of the order of several m/s per 100 m can be developed in this way; significantly greater shears would be expected to break down due to turbulence because of Richardson's Criterion.

At the present our knowledge of the behavior of inertial, or quasi-inertial, oscillations in an Eulerian coordinate system, their horizontal extent, their rate of propagation and their changes in time and space, is very limited. Yet, the implications of the observed mesostructure are such that they warrant exhaustive study. Not only may the observed details in wind profiles adversely affect vertically rising launch vehicles, but the combination of excessive shears with small values of thermal stability may produce localized regions of turbulent flow, producing the hazard of clear-air turbulence for horizontally flying sub- or supersonic aircraft. In this report only a simple forecast scheme for predicting maximum shears is given. The persistence of phenomena at these altitudes, and the lack of local terrain and heat sources which complicate low level meteorology, suggest that eventually improved data acquisition and improved understanding will permit a high accuracy in forecasting.

Future research should be designed to explore the physical nature of the observed mesostructural details in the wind field. This can be done only if atmospheric parameters other than wind are included in the study to the same degree of detail as presently offered by FPS-16 soundings. Temperature and pressure -- a combination of which yields potential temperature -- appear to be the most important of these parameters, and turbulence would also prove to be a valuable measurement. The generally dry environment of the stratosphere, in

which most of the observed wind fluctuations occur, would allow the assumption that potential temperatures are conserved by air parcels over an appreciable period of time. Thus, wind fluctuations could be mapped accurately not only with respect to height, but with respect to a "physical" surface of constant potential temperature (constant entropy), along which the perturbations would actually travel. Such added capabilities of analysis would greatly enhance our means of estimating the persistence, the predictability, and the general physical nature of the atmospheric mesostructure.

An effort should be made to extend the present studies from their single-station confinement to an area coverage. One approach would be to employ, in addition to the FPS-16 ascent series, constant-level balloons drifting at various altitudes, possibly in the vicinity of observed wind speed maxima and minima. However, the difficulty of establishing and maintaining exact altitudes or constant entropy surfaces for the balloons should be recognized. Errors of a few hundred meters could mask the desired data because of the strong vertical variations of speed. Another approach is to make detailed measurements of winds and temperatures by aircraft, conducted simultaneously with FPS-16 soundings. This would enable us to study the advective properties of mesostructural phenomena, at least within selected layers. The persistence of structural details, evident from the radar tracking of balloons, suggests that wind speed anomalies extend over large distances measured along the upper current. Analyses of Project Jet Stream Data (Reiter, 1962) indicate that the dimensions of such details may be much shorter when measured across the direction of flow. These aircraft data have mainly been collected along horizontal flight legs. If measurements were made along isentropic surfaces, which are sloping in space where the basic current shows vertical shears, the mesostructure may present a different picture altogether. It might very well be possible that wind fluctuations observed in FPS-16 soundings, as well as in Project Jet Stream Flights, align themselves in wide and long, but shallow, "sheets" parallel to isentropic surfaces.

None of these speculations, or the ones presented earlier in this report, can be substantiated without additional measurement data. The design of the experiment should be changed, however, to incorporate other basic atmospheric parameters to the same degree of resolution as the vertical wind profiles discussed here.

APPENDIX A

TABLES OF PERCENTAGE FREQUENCY OF OCCURRENCE OF SHEARS AND THE DEPTHS THROUGH WHICH THEY WERE ACTIVE

Wind Speed Shear (mps/100 m)	California												Averages				Florida			
	June 5	June 19	June 20	Aug. 27	Aug. 27	Sept. 10	Oct. 2	Oct. 16	Dec. 4	Dec. 12	Dec. 26	Jan. 28	Cyclonic	Anti-Cyclonic	Post-Cyclonic	All Cases	Jan. 3	Mar. 18	All Cases	
0-0.99	+ 3.5	10.9	10.9	8.5	10.4	17.9	7.9	15.0	10.7	12.5	5.0	5.0	5.7	11.7	10.2	11.3	10.1	12.2	11.1	11.1
	- 2.9	13.3	20.8	8.0	4.9	14.0	15.8	17.3	7.0	13.6	5.9	5.9	9.4	10.2	10.1	11.9	8.4	17.1	17.1	12.1
1.0-1.99	+ 13.5	16.9	20.8	19.5	28.8	20.3	28.6	25.7	19.7	25.0	25.4	25.4	21.1	21.2	23.6	12.9	29.6	30.5	30.0	30.0
	- 12.3	13.9	21.8	19.0	20.2	21.0	26.8	25.0	26.2	14.7	23.7	23.7	19.5	19.1	25.0	12.9	29.4	23.2	27.1	27.1
2.0-2.99	+ 10.0	12.7	13.9	16.0	10.4	9.3	9.6	5.3	13.1	8.5	11.0	11.0	9.8	12.5	9.8	11.7	10.9	3.7	8.0	8.0
	- 11.7	12.7	9.9	12.5	17.1	10.9	5.5	5.7	15.9	14.2	11.8	11.8	8.6	12.6	11.1	12.1	7.6	9.8	8.5	8.5
3.0-3.99	+ 6.4	4.8	2.9	3.0	1.2	1.5	2.4	2.6	3.2	1.7	5.9	5.9	4.4	2.7	3.9	6.3	0.8	0.0	0.5	0.5
	- 8.8	6.0	1.9	4.0	2.4	3.1	1.0	0.3	1.8	5.1	5.0	5.0	4.9	3.5	2.4	3.5	0.0	3.7	1.5	1.5
4.0-4.99	+ 2.9	1.2	1.4	2.0	0.6	0.0	1.0	0.3	0.4	0.5	2.5	2.5	2.0	1.0	1.1	1.3	0.8	0.0	0.5	0.5
	- 4.1	1.8	1.9	1.0	1.2	0.0	0.6	0.7	0.9	3.9	1.6	1.6	2.4	1.2	1.1	1.7	0.8	0.0	0.5	0.5
5.0-5.99	+ 4.1	0.6	0.0	0.5	0.6	0.0	0.0	0.3	0.4	0.0	0.8	0.8	2.0	0.3	0.5	0.7	0.0	0.0	0.0	0.0
	- 3.5	1.8	0.4	2.0	0.0	0.7	0.0	0.7	0.0	0.0	0.8	0.8	1.8	1.0	0.5	0.9	0.0	0.0	0.0	0.0
6.0-6.99	+ 1.7	1.2	0.4	2.0	0.0	0.0	0.0	0.3	0.0	0.0	0.0	0.0	0.9	0.7	0.1	0.6	0.0	0.0	0.0	0.0
	- 1.1	0.0	0.9	0.0	1.2	0.0	0.0	0.0	0.0	0.0	0.0	0.0	0.6	0.4	0.0	0.3	0.0	0.0	0.0	0.0
7.0-7.99	+ 0.5	0.6	0.0	0.0	0.0	0.7	0.3	0.0	0.0	0.0	0.0	0.0	0.4	0.3	0.0	0.2	0.0	0.0	0.0	0.0
	- 1.1	0.0	0.9	0.0	0.0	0.0	0.0	0.0	0.0	0.0	0.0	0.0	0.6	0.2	0.0	0.2	0.8	0.0	0.5	0.5
8.0-8.99	+ 1.7	0.0	0.0	1.0	0.6	0.0	0.0	0.0	0.0	0.0	0.0	0.0	0.9	0.3	0.0	0.3	0.0	0.0	0.0	0.0
	- 0.5	0.0	0.0	0.0	0.0	0.0	0.0	0.0	0.0	0.0	0.0	0.0	0.3	0.0	0.0	0.1	0.0	0.0	0.0	0.0
9.0-9.99	+ 0.5	0.0	0.0	0.0	0.0	0.0	0.0	0.0	0.0	0.0	0.0	0.0	0.3	0.0	0.0	0.2	0.0	0.0	0.0	0.0
	- 2.3	0.0	0.0	0.0	0.0	0.0	0.0	0.0	0.0	0.0	0.0	0.0	1.2	0.0	0.0	0.2	0.0	0.0	0.0	0.0
> 10.0	+ 2.9	0.6	0.0	0.5	0.0	0.0	0.0	0.0	0.0	0.0	0.0	0.0	1.5	0.1	0.0	0.3	0.0	0.0	0.0	0.0
	- 2.9	0.6	0.0	0.0	0.0	0.0	0.0	0.0	0.0	0.0	0.0	0.0	1.5	0.2	0.0	0.4	0.0	0.0	0.0	0.0
50	15.3	10.0	5.5	7.5	5.5	4.6	9.6	13.0	6.5	6.2	11.0	11.0	12.5	6.6	10.2	8.7	5.0	8.5	6.5	6.5
100	17.1	19.0	13.9	17.0	18.1	11.7	21.7	17.3	13.6	22.7	15.2	15.2	19.4	15.9	15.4	17.3	13.4	26.8	19.1	19.1
150	15.3	16.2	14.4	13.0	8.5	10.9	11.0	10.3	10.7	7.3	11.0	11.0	13.2	12.6	10.7	11.6	10.1	13.4	11.6	11.6
200	14.1	15.8	12.4	17.5	19.6	21.0	14.4	14.6	12.2	8.5	14.4	14.4	14.3	17.3	13.7	14.7	12.6	24.4	17.1	17.1
250	7.1	7.7	9.4	8.5	7.3	7.8	13.1	10.7	7.9	8.5	10.1	10.1	10.1	8.2	9.6	9.2	8.4	3.7	6.5	6.5
300	7.6	11.3	19.9	6.5	9.8	14.0	10.6	8.8	9.8	6.2	8.4	8.4	9.1	10.6	9.0	9.4	6.7	11.0	8.5	8.5
350	3.5	6.9	5.9	6.0	6.7	4.6	3.1	3.8	5.1	3.9	5.0	5.0	3.3	6.0	4.6	4.8	3.4	1.2	2.5	2.5
400	4.7	4.1	4.4	6.0	7.9	6.2	4.8	6.5	9.3	1.1	2.5	2.5	3.8	5.7	6.1	5.4	6.7	3.7	5.5	5.5
450	0.6	3.1	4.9	2.0	0.6	4.6	3.1	3.4	3.2	4.5	6.7	6.7	1.9	3.0	4.4	3.3	4.2	3.7	4.0	4.0
500	4.7	1.8	4.9	4.0	3.0	5.4	2.4	3.4	3.2	3.4	5.0	5.0	3.6	4.1	3.9	3.7	10.9	4.9	8.5	8.5
550	1.8	1.8	0.9	2.0	3.0	1.5	1.7	0.3	1.4	0.5	0.8	0.8	1.8	1.8	0.8	1.4	3.4	2.4	3.0	3.0
600	2.9	1.8	2.9	2.5	2.4	0.0	1.7	1.9	3.7	3.4	3.3	3.3	2.3	1.9	3.0	2.4	3.4	4.9	4.0	4.0
650	2.9	0.6	1.4	1.5	1.2	2.3	1.3	2.3	2.3	0.5	0.8	0.8	2.1	1.4	1.8	1.6	1.7	0.0	1.0	1.0
700	0.6	0.6	0.9	0.0	0.6	1.5	0.3	1.5	0.9	2.8	3.3	3.3	0.5	0.7	1.9	1.1	0.8	0.0	0.5	0.5
750	1.2	1.7	0.9	0.5	1.2	0.7	0.3	0.7	0.4	2.8	0.0	0.0	0.8	1.0	0.4	1.0	5.0	0.0	3.0	3.0
800	0.0	0.0	0.9	1.0	0.6	0.0	0.6	0.3	2.3	1.1	0.0	0.0	0.3	0.5	0.9	0.8	0.8	0.0	0.5	0.5
850	0.6	0.0	0.4	0.0	0.0	0.0	0.3	0.3	0.4	0.0	0.0	0.0	0.5	0.1	0.2	0.2	1.7	0.0	1.0	1.0
900	0.0	0.6	0.4	1.5	1.8	0.7	0.3	0.0	0.9	0.5	0.0	0.0	0.2	1.0	0.3	0.6	0.8	0.0	0.5	0.5
950	0.0	0.0	0.9	0.0	1.2	0.7	0.0	0.3	0.9	0.0	0.0	0.0	0.0	0.6	0.4	0.4	0.0	0.0	0.0	0.0
1000	0.0	0.0	1.4	1.5	0.0	0.7	0.0	0.0	1.4	1.7	0.8	0.8	0.0	0.7	0.7	0.7	0.0	0.0	0.0	0.0
> 1000	0.0	0.0	0.4	0.5	6.1	1.4	0.0	0.3	0.4	12.2	0.0	0.0	0.0	1.7	0.2	1.9	0.8	0.0	0.5	0.5

APPENDIX A (continued)

	California										Averages				Florida			
	June 5	June 19	Aug. 20	Aug. 27	Sept. 10	Oct. 2	Oct. 16	Dec. 4	Dec. 12	Dec. 26	Jan. 28	Cyclonic	Anti-Cyclonic	Post-Cyclonic	All Cases	Jan. 3	Mar. 18	All Cases
0-4.99	+ 11.9	22.5	20.5	11.7	18.4	20.1	2.6	16.2	25.2	40.7	11.1	7.3	18.6	17.5	16.6	43.8	45.6	44.3
-	13.8	21.7	19.0	11.0	16.5	11.2	8.6	11.5	18.8	39.4	15.1	11.2	15.8	15.0	18.1	34.9	45.6	37.9
5.0-9.99	+ 17.6	12.0	13.5	18.6	14.5	14.5	16.6	23.5	17.7	8.2	21.2	17.1	14.6	20.8	16.7	7.5	5.3	6.9
-	15.0	8.8	17.5	15.8	11.6	14.5	18.6	20.9	19.8	9.5	20.2	16.8	13.6	20.3	16.9	12.3	3.5	9.9
10.0-14.99	+ 6.9	1.6	5.5	5.5	8.7	4.8	6.6	8.3	3.7	1.2	5.0	6.8	5.2	5.7	5.5	0.7	0.0	0.5
-	9.4	4.0	3.5	6.8	6.7	5.6	12.6	9.9	6.9	3.1	5.0	11.0	5.3	6.0	7.1	0.0	0.0	0.0
15.0-19.99	+ 4.4	0.8	3.5	2.7	1.9	4.0	9.3	1.0	0.0	0.0	5.0	6.9	2.5	2.0	3.0	0.7	0.0	0.5
-	3.7	3.2	3.0	5.5	1.9	4.8	6.0	4.7	1.6	0.0	3.0	4.9	3.6	3.1	3.6	0.0	0.0	0.0
20.0-24.99	+ 2.5	1.6	2.0	2.7	1.9	3.2	3.3	0.5	0.0	0.0	0.0	2.9	2.6	0.2	1.8	0.0	0.0	0.0
-	1.8	1.6	1.0	2.0	2.9	1.6	2.6	1.0	0.5	0.0	1.0	2.2	1.8	0.8	1.5	0.0	0.0	0.0
25.0-29.99	+ 1.2	1.6	0.0	2.7	1.9	2.4	0.0	0.0	0.5	0.0	0.0	1.6	0.8	0.5	0.8	0.0	0.0	0.0
-	0.6	0.8	0.0	1.3	1.9	0.8	0.6	0.0	0.0	0.0	0.0	0.3	1.8	0.2	1.0	0.0	0.0	0.0
30.0-34.99	+ 0.0	0.8	2.0	2.7	2.9	1.6	1.3	0.0	0.0	0.0	3.0	0.7	2.0	1.0	1.2	0.0	0.0	0.0
-	1.2	0.0	0.0	0.0	0.0	0.0	1.3	0.0	0.0	0.0	0.0	1.3	0.0	0.0	0.3	0.0	0.0	0.0
35.0-39.99	+ 1.8	0.0	1.0	0.0	2.9	2.4	1.3	0.5	0.0	0.0	0.0	1.6	1.3	0.2	0.9	0.0	0.0	0.0
-	1.2	2.4	0.0	0.0	0.9	1.6	0.6	0.0	0.0	0.0	0.0	0.9	1.0	0.0	0.6	0.0	0.0	0.0
40.0-44.99	+ 1.2	2.4	0.0	0.7	0.9	0.8	0.6	0.0	0.0	0.0	1.0	0.9	1.0	0.3	0.6	0.0	0.0	0.0
-	1.2	0.0	0.5	0.7	0.9	0.0	0.0	0.0	0.0	0.0	0.0	0.6	0.4	0.0	0.3	0.0	0.0	0.0
45.0-49.99	+ 1.2	0.0	0.5	0.7	0.0	0.8	0.6	0.0	0.0	0.0	0.0	0.9	0.4	0.0	0.4	0.0	0.0	0.0
-	1.2	4.8	2.0	0.7	0.0	0.8	0.0	0.0	0.0	0.0	0.0	0.6	1.7	0.0	0.9	0.0	0.0	0.0
≥ 50.0	+ 0.6	4.0	1.5	4.8	1.9	2.4	2.0	0.0	0.5	0.0	3.0	1.3	2.9	1.2	1.8	0.0	0.0	0.0
-	22.6	8.0	6.5	5.5	2.9	4.8	0.0	2.6	8.0	5.7	5.0	11.3	5.5	5.2	6.7	8.9	10.5	9.4
50	15.0	16.1	15.5	18.5	10.6	13.8	9.3	9.9	17.7	20.3	22.2	12.2	14.8	16.6	15.2	25.7	26.3	25.1
100	10.0	12.0	14.5	10.4	6.7	9.6	12.0	13.6	9.6	10.1	14.1	11.0	10.6	12.4	11.4	9.6	10.5	9.9
150	11.3	21.7	16.0	11.8	12.6	10.4	14.0	10.4	12.9	10.1	15.1	12.7	14.5	12.8	13.2	11.6	10.5	11.3
200	10.0	9.6	11.0	8.3	18.4	12.9	17.3	5.7	8.0	5.0	7.0	13.7	12.0	6.9	10.0	9.6	10.5	9.9
250	11.3	8.0	11.5	9.7	11.6	18.5	13.3	12.5	5.3	13.3	3.0	12.3	11.9	6.9	10.9	9.6	7.0	8.9
300	2.5	6.4	3.5	6.2	6.7	4.0	4.0	12.5	6.4	3.8	7.0	2.3	5.4	8.6	5.8	2.1	0.0	1.5
350	4.4	5.6	6.5	9.7	4.8	5.6	6.6	5.2	5.3	5.0	6.0	5.0	6.4	5.5	5.9	1.4	0.0	1.0
400	1.8	4.0	3.5	1.3	5.8	3.2	2.6	5.2	1.6	0.6	6.0	2.2	3.6	4.3	3.1	2.7	1.8	2.5
450	3.7	1.6	4.0	6.2	3.8	9.6	8.0	5.7	9.6	2.5	5.0	5.9	5.0	6.8	5.6	6.2	1.8	4.9
500	1.2	2.4	1.0	0.6	3.8	1.6	3.3	3.1	2.1	1.2	1.0	2.3	2.1	2.1	2.0	1.4	0.0	1.0
550	0.6	2.4	1.5	2.7	1.9	0.8	2.6	1.0	5.3	1.2	4.0	1.6	1.9	3.4	2.2	5.5	3.5	4.9
600	1.8	1.6	1.0	1.3	2.9	0.8	0.6	4.1	1.6	0.6	1.0	1.2	1.5	2.2	1.7	1.4	0.0	1.0
650	0.7	0.0	2.0	2.7	0.9	0.8	2.0	2.6	1.0	4.4	3.0	1.4	1.3	2.2	1.9	2.7	3.5	3.0
700	0.7	0.0	1.0	1.3	1.9	0.0	2.6	2.0	0.5	3.1	0.0	1.7	0.8	0.8	1.3	0.7	0.0	0.5
750	1.2	0.0	0.0	0.6	0.0	1.6	0.6	0.5	1.0	3.8	0.0	0.9	0.4	0.5	0.9	0.7	1.8	1.0
800	0.7	0.0	0.5	0.6	0.9	0.8	0.0	0.0	0.5	0.6	0.0	0.4	0.6	0.2	0.4	0.0	1.8	0.5
850	0.0	0.0	0.0	1.3	0.9	0.8	0.6	2.0	1.6	3.1	0.0	0.3	0.6	1.2	1.0	0.7	3.5	1.5
900	0.0	0.0	0.0	0.6	0.0	0.0	0.0	0.0	0.5	0.0	0.0	0.0	0.0	0.2	0.1	0.0	1.8	0.5
950	0.0	0.0	0.0	0.6	0.0	0.0	0.0	0.0	0.5	0.0	0.0	0.0	0.0	0.3	0.1	0.0	1.8	0.5
1000	0.7	0.0	0.5	0.0	1.9	0.0	0.0	0.5	0.5	4.4	0.0	0.4	0.5	0.3	0.7	1.4	5.3	3.0

Wind Direction Shear (deg/100 ft)

Depth of Wind Direction Shear (meters)

APPENDIX B

Δv	< 1.0		1.0 - 1.9		2.0 - 2.9		3.0 - 3.9		4.0 - 4.9		5.0 - 5.9		6.0 - 6.9		7.0 - 7.9		8.0 - 8.9		9.0 - 9.9		≥ 10.0		TOTAL	
	Δz	+	-	+	-	+	-	+	-	+	-	+	-	+	-	+	-	+	-	+	-	+	-	+
50	1.10	1.25	1.85	1.45	.95	.75	.40	.20	.35	.05	-	.10	.15	.20	.05	-	.05	-	-	-	.10	-	5.00	4.00
	1.50	1.00	1.00	2.00	1.00	1.00	-	-	-	-	-	-	-	-	-	-	-	-	-	-	-	-	2.50	4.00
100	1.40	1.60	4.30	2.35	3.40	1.50	1.30	.70	.25	.40	.10	.15	.20	.10	.05	-	.05	-	-	.10	.05	.05	11.05	7.00
	1.00	1.00	7.00	8.00	8.00	8.00	-	-	-	-	-	-	-	-	-	1.50	-	-	-	-	-	-	10.00	8.00
150	.75	.45	2.05	2.05	1.65	1.15	.60	1.10	.30	.65	.25	.15	.05	.15	-	-	.10	.10	-	.10	.05	.10	6.50	6.00
	.60	.80	2.00	2.00	2.00	2.00	1.00	.50	-	-	-	-	-	-	-	-	-	-	-	-	-	-	6.50	6.00
200	.30	.15	1.35	1.70	2.00	1.70	1.30	1.30	1.40	1.25	.75	.55	.20	.35	.20	.20	.15	.20	.05	.05	.10	.05	7.00	7.50
	-	1.50	1.00	2.00	2.00	2.00	2.50	2.00	1.00	.50	-	-	-	-	-	-	-	-	-	-	-	-	7.00	8.50
250	.20	.05	.60	.40	.80	1.10	1.35	.90	.45	.90	.65	.65	.40	.35	.10	.10	.05	.30	.10	-	.05	.05	6.75	4.00
	-	.50	1.00	.50	1.50	2.00	.50	.50	-	-	.50	-	.50	-	-	-	-	-	-	-	-	-	6.00	2.00
300	.10	.10	.25	.55	.65	.65	.85	1.20	.45	.70	1.05	.75	.35	.50	.20	.30	.10	.15	.10	.15	.05	.50	4.15	5.55
	-	1.00	-	.50	1.50	1.50	1.50	2.50	1.50	.50	.50	.50	-	-	-	-	-	-	-	-	-	-	4.00	6.00
350	.05	-	.20	.15	.25	.20	.35	.15	.25	.35	.75	.35	.30	.20	.25	.40	.25	-	-	.10	.25	.25	2.90	2.15
	-	-	.50	-	-	-	.50	-	-	-	1.00	.50	-	-	-	-	-	-	-	-	-	-	1.50	1.00
400	-	-	.05	.15	.25	.15	.35	.35	.75	.35	.45	.45	.25	.55	.10	.25	.15	.30	.15	.25	.10	.30	2.60	3.10
	-	-	.50	.50	-	-	.50	-	-	.50	-	.50	.50	1.00	.50	-	.50	-	-	-	.50	.50	2.50	2.00
450	-	.05	.05	-	.15	.10	.20	.20	.10	.10	.35	.10	.05	.40	.25	.40	.15	.10	.10	.10	.10	.35	1.50	1.90
	-	-	-	-	-	-	-	-	.50	-	-	-	.50	-	-	.50	-	-	1.00	.50	.50	.50	2.50	2.50
500	-	-	-	.10	.10	.10	.30	.15	.15	.10	.10	.40	.20	.10	.35	.50	.20	.05	.25	.20	.35	1.70	2.10	
	-	-	-	.50	1.00	1.00	1.50	1.00	1.00	1.00	1.00	1.00	1.00	1.00	1.00	1.00	1.00	1.00	1.00	1.00	1.00	1.00	4.00	6.00
550	-	-	-	.05	-	-	.15	-	.05	.05	-	.10	.10	.15	.05	.20	.10	.05	.05	.05	.25	.35	.60	1.15
	-	-	-	.50	-	-	.50	-	.50	-	-	.50	1.00	.50	1.00	.50	.50	.50	.50	.50	1.00	1.00	.50	2.50
600	-	-	-	-	.10	-	.10	.05	-	-	.05	.10	.05	.30	.20	.20	.05	.20	.10	.20	.35	.50	1.00	1.55
	-	-	-	-	-	-	.50	-	-	-	.50	-	.50	-	.50	-	.50	-	.50	.50	.50	-	2.00	2.00
650	.05	-	-	-	-	-	-	-	.05	.05	.15	.15	.25	.05	.05	.05	.15	.05	.05	.10	.25	.15	.95	.60
	-	-	-	-	-	-	-	-	-	-	-	-	1.00	-	-	-	-	-	-	-	-	-	1.00	-
700	-	-	-	-	-	-	.05	.10	-	-	.05	.05	-	.10	.05	-	.10	.05	.05	.15	.05	.45	.35	.90
	-	-	-	-	-	-	-	-	-	-	-	-	-	-	-	.50	-	-	-	-	-	-	.50	-
750	-	-	-	-	-	.05	-	-	-	-	.05	-	.15	.15	.10	.05	.10	.10	-	-	.10	.20	.50	.55
	-	-	-	-	-	-	-	-	-	-	-	-	-	-	-	-	.50	.50	-	-	.50	2.00	2.50	
800	-	-	-	.05	-	-	-	-	-	.05	-	.05	-	.05	-	.05	.10	-	-	-	.10	.30	.25	.45
	-	-	-	-	-	-	-	-	-	-	-	-	-	-	-	-	-	-	-	-	.50	-	.50	
850	-	-	-	-	-	-	-	-	-	-	-	-	-	-	-	.05	.05	.05	.05	-	.15	.05	.20	
	-	-	-	-	-	-	-	-	-	-	-	-	.50	-	-	-	.50	-	.50	-	.50	1.00	1.00	
900	-	-	-	-	-	-	-	-	-	.05	.05	.05	-	-	-	.50	-	-	.05	.05	.10	.25	.20	.40
	-	-	-	-	-	-	-	-	-	-	-	-	-	-	-	-	-	-	-	-	-	-	.50	
950	-	-	-	-	-	-	-	-	-	-	-	-	.05	-	-	-	.05	-	.05	-	.05	.20	.15	.25
	-	-	-	-	-	-	-	-	-	-	-	-	-	-	-	-	-	-	-	-	-	-	-	
≥ 1000	-	-	-	-	-	-	-	-	-	-	-	-	.05	-	-	.15	.10	.05	-	-	.90	1.30	1.05	1.50
	-	-	-	-	-	-	-	-	-	-	-	-	-	-	-	.50	.50	-	-	-	.50	.50	.50	.50
TOTAL	3.95	3.65	11.50	9.00	10.30	7.45	6.95	6.70	6.55	5.05	4.80	3.80	3.10	4.00	1.75	2.70	2.20	2.00	.95	1.65	3.20	6.45		
	2.00	2.50	14.00	14.00	11.00	8.50	8.50	8.00	4.00	1.50	2.00	2.00	2.50	1.50	2.50	4.50	1.50	.50	2.00	2.00	2.00	2.00	2.00	2.00

JOINT EMPIRICAL PROBABILITY DISTRIBUTION OF WIND SPEED CHANGE (Δv) AND DEPTH OF THE CHANGE LAYER (Δz)

Probability in per cent of the total observations (2088 in California - Gothic numerals; 206 in Florida - Italic numerals). Statistics can be converted to empirical probability on a given day by multiplying by 190 (California) or 200 (Florida). Empirical probability on an individual sounding is derived by multiplying by 20 (California) or 8 (Florida). Probabilities greater than 100 per cent indicate more than one occurrence.

REFERENCES

- Avsec, D., 1939: Thermoconvective Eddies in Air; Application to Meteorology, Sci. and Tech. Publ. of Air Ministry Works, Inst. of Fluid Mech., Fac. of Sci., Paris, No. 155. Translated from French by C. Ronne, Woods Hole Ocean. Inst., Woods Hole, Mass.
- Bigg, E. K., 1964: Atmospheric Stratification Revealed by Twilight Scattering, *Tellus*, 16, 1, pp. 76-83.
- Blackadar, A. K., 1957: Boundary Layer Wind Maxima and their Significance for the Growth of Nocturnal Inversions. *Bull. Am. Meteorol. Soc.*, 38, pp. 283-290.
- Brunt, D., 1939: *Physical and Dynamical Meteorology*, Cambridge Univ. Press, New York, 428 pages.
- Conover, J. H., 1960: Cirrus Patterns and Related Air Motions Near the Jet Stream as Derived by Photography, *J. Meteorol.*, 17, pp. 532-546.
- Danielsen, E. F., 1959: The Laminar Structure of the Atmosphere and its Relation to the Concept of a Tropopause, *Arch. Meteorol. Geophys. Bioklimatol., Serie A: Meteorologie und Geophysik*, Band 11, 3. Heft.
- Danielsen, E. F., 1964: Confirmation of Mass Transport as a Form of Stratospheric-Tropospheric Exchange, Program of Amer. Met. Soc., 44th Annual Meeting, January 29-31, Los Angeles, California, p. 716.
- Hines, C. O., 1960: Internal Atmospheric Gravity Waves at Ionospheric Heights, *Can. J. Phys.*, 38, pp. 1441-1468.
- Kroening, J. L., and E. P. Ney, 1962: Atmospheric Ozone, *J. Geophys. Res.*, 67, 5, pp. 1867-1875.
- Kuettner, J., 1959: The Band Structure of the Atmosphere, *Tellus*, 11, 3, p. 267.

- MacCready, P. B., and Henry R. Jex, 1964: Study of Sphere Motion and Balloon Wind Sensors. Final Report to NASA, Huntsville, Ala. Contract NAS 8-5294. NASA TM X-53089.
- Mee, T. R., 1964: An Investigation of Convective Cells Over the Ocean, Meteorology Research, Inc., Final Report to Applied Oceanography Group, Scripps Institution of Oceanography, Contract SD 75543-0.
- Murrow, Harold N., and Robert M. Henry, 1965: Self-Induced Balloon Motions, J. Appl. Meteorol., 4, 1, pp. 131-138.
- Newton, C. W., 1959: Axial Velocity Streaks in the Jet Stream: Ageostrophic "Inertial" Oscillations, J. Meteorol., 16, 6, pp. 638-645.
- Pack, D., 1962: Air Trajectories and Turbulence Statistics from Weather Radar Using Tetroons and Radar Transponders, Monthly Weather Rev., 90, pp. 491-506.
- Raethjon, P., 1958: Traegheitsellipse und Jet Stream, Geophysica Helsinki, 6, 3, pp 439-453.
- Reiter, E. R., 1962: Die vertikale Struktur des Strahlstromkernes aus Forschungsflügen des Project Jet Stream, Berichte d. Deutsch. Wetterdienstes, Nr. 80, Band 11, 30 pp.
- _____, 1963: A Case Study of Radioactive Fallout, J. Appl. Meteorol., 2, 6, pp. 691-705.
- Reiter, E. R., and J. D. Mahlman, 1964: Heavy Radioactive Fallout Over the Southern United States, November, 1962, from Transport Processes in the Atmosphere Leading to Radioactive Fallout, Colorado State University, Dept. of Atmospheric Science, Tech. Paper No. 58, pp. 21-50.
- Sawyer, J. S., 1961: Quasi-Periodic Wind Variations with Height in the Lower Stratosphere, Quart. J. Roy. Meteorol. Soc., 87, 371, p. 24.
- Scoggins, James R., 1964: Aerodynamics of Spherical Balloon Wind Sensors, J. Geophys. Res., 69, 4, pp. 591-598.
- _____, 1965: Spherical Balloon Wind Sensor Behavior, J. Appl. Meteorol., 4, 1, pp. 139-145.

Smith, T. B., And M. A. Wolf, 1963: Vertical Diffusion from an Elevated Line Source Over a Variety of Terrains, Meteorology Research, Inc., Final Report, Part A, to Dugway Proving Ground, Contract DA-42-007-CML-545. AD 418 599.

Stinson, J. R., A. I. Weinstein, and E. R. Reiter, 1964: Details of Wind Structure from High Resolution Balloon Soundings, Report on Contract NAS8-5294, NASA TMX-53115, August 1964, Huntsville, Alabama.

Woodcock, A. H., 1942: Soaring over the Open Sea, Scientific Monthly, September, pp. 226-232.

June 28, 1965

APPROVAL

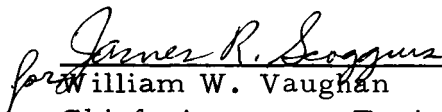
NASA CR-61080

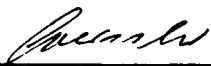
MESOSCALE STRUCTURE OF 11-20 KM WINDS

By A. I. Weinstein and E. R. Reiter

The information in this report has been reviewed for security classification. Review of any information concerning Department of Defense or Atomic Energy Commission programs has been made by the MSFC Security Classification Office. This report, in its entirety, has been determined to be unclassified.

This document has also been reviewed and approved for technical accuracy.


for William W. Vaughan
Chief, Aerospace Environment Office


E. D. Geissler
Director, Aero-Astroynamics Laboratory

DISTRIBUTION

INTERNAL

Dep Dir Technical
Dr. Rees

R&D Operations
Mr. Weidner
Mr. Dannenburg/Dr. Kuettner

R-AERO

Dr. Geissler
Mr. O. C. Jean
Mr. R. Cummings
Mr. H. Horn
Mr. C. Baker
Dr. F. Speer
Mr. J. Lindberg
Mr. L. Stone
Mr. T. Reed
Mr. J. de Fries
Mr. L. McNair
Mr. W. K. D hm
Mr. M. Rheinfurth
Mr. F. Kurtz
Mr. J. Sheats
Mr. C. Fulmer
Mr. E. Linsley
Dr. Heybey
Mr. H. Wilson
Mr. O. Holderer
Mr. M. J. Hart
Mr. J. Winch
Mr. R. Ryan
Mr. R. Lewis
Mr. G. E. Daniels
Mr. O. E. Smith
Mr. J. Kaufman
Mr. W. W. Vaughan (20)
Mr. J. R. Scoggins (40)

Research Projects-DIR

R-P&VE-DIR

Mr. H. Palaoro
Mr. N. Showers
Mr. R. Hunt
Mr. J. Moore
Mr. G. Kroll
Mr. E. Goerner

R-ASTR-DIR

Mr. H. Hosenthien
Mr. H. Mink
Mr. Blackstone
Mr. O. Hoberg
Mr. J. Boehm

R-COMP

Mr. D. G. Aichele
Mr. P. Harness
Mr. F. Herring
Mr. R. Craft
Miss L. Smith

R-TEST-DIR

LVO-DIR

MS-IPL (8)

MS-IP

I-RM-M

PAT

MS-H

CC-P

MS-T (5)

Industrial Operations

S-IB Mr. L. James

S-V Dr. Rudolph

MISS. TEST OPERATIONS

Mr. L. W. Nybo

DISTRIBUTION (CONT'D)

Kennedy Space Flight Center

Dr. Debut (2)
Dr. H. Gruene
Dr. A. Knothe
Dr. R. Bruns (3)
L/Col. Patrone
Mr. J. Simmons
Mr. D. Collins
Mr. Poppel/Mr. Buchanan
Mr. . Taiani
Mr. J. Deese
Mr. G. von Tiesenhausen
Col. A. Gibbs
Mr. W. Jelen
Mr. K. Sandler
Mr. Albert Zeiler

Army Missile Command

Library
Dr. Essenwanger

DISTRIBUTION (CONT'D)

EXTERNAL

Manned Spacecraft Center (NASA)
Houston, Texas

ATTN: Director (2)
Dr. J. M. Eggelston
Mr. Thompson

Manned Spacecraft Center (NASA)
Cape Kennedy Florida

Research Apollo Spacecraft
Projects Office
Mr. Jerry Valek

Langley Research Center (NASA)
Langley Station, Hampton, Virginia

Mr. H. B. Tolefson
Mr. Vernon Alley
Mr. R. M. Henry
Mr. W. H. Reed, III
Mr. Harry Runyan
Library

Pan American, Patrick
Air Force Base, Florida
Division Meteorologist

Weather Bureau, U. S. Dept. of
Commerce, Washington, D. C.

Dr. R. M. White, Chief
Dr. H. E. Landsberg
Mr. K. Nagler

Pacific Missile Range
Point Mugu, California

Mr. John Masterson
Code 3101-1.1

National Weather Records Center
Asheville, North Carolina

Dr. Barger
Dr. Crutcher

NASA Headquarters
Washington, D. C.

Tracking and Data Acquisition Office
Mr. T. Buckley
Office of Advanced Research and
Technology

Mr. R. Rhode, RVA
Mr. D. Gilstad, RV-2 (2)
Dr. A. Kelley, RE

Space Sciences and Application
D. M. Tepper
D. H. Newell

Office of Manned Space Flight
Gemini Program Director
Apollo Program Director
Advanced Mission Program Director

Commander (2)
Air Weather Service
Scott Air Force Base, Illinois

Air Force Cambridge Research
Laboratories, Code: CREW
L. G. Hanscon Field

Bedford, Massachusetts

Mr. N. Sissenwine
Dr. M. Barad
Mr. R. Levitan

Lt. Dan Reid
Mr. R. Slavin
Dr. D. Haugen
Technical Library

Manned Spacecraft Center (NASA)
Houston, Texas

Apollo Project Office Director
Weather Support Group
Mr. D. Wade

DISTRIBUTION (CONT'D)

EXTERNAL (CONT'D)

Air Force System Command (2)
Code: SCWTS
Andrews Air Force Base
Washington, D. C. 20331

Mr. George Muller
Air Force Flight Dynamic Laboratory
Air Force System Command
Wright Patterson Air Force Base, Ohio

Mr. William Elam
Bellcom, Inc.
1100 17th Street, N. W.
Washington 6, D. C.

Air Force Systems Command
Space System Division
Air Force Unit Post Office
Los Angeles, California

Meteorological & Geostrophical
Abstracts
P. O. Box 1736
Washington, D. C.

Mr. Richard Martin
General Dynamics Astronautics
San Diego, California

Mr. Carl Wentworth
NASA-Lewis Research Center
2100 Brookpark Road
Cleveland, Ohio

Mr. Robert Borland
Apollo Support Department
General Electric Company
P. O. Box 26287
Houston, Texas

Mr. John Mayer, Chief
Mission Analysis Division
NASA-Manned Spacecraft Center
Houston, Texas

Mr. Marvin White
Space Technology Laboratories, Inc.
Structures Department
One Space Park
Redondo Beach, California

Chrysler Corporation
S-I Project Director (2)
THRU: MSFC Saturn Systems Office

Scientific and Technical Information
Facility (25)
ATTN: NASA Representative (S-AK/RKT)
P. O. Box 5700
Bethesda, Maryland

Dr. Elmar Reiter (25)
Dept. of Atmospheric Science
Colorado State University
Fort Collins, Colorado

Dr. J. R. Stinson
U.S. Navy Weather Research Facility
Norfolk, Virginia

Meteorology Research, Inc.
2420 N. Lake Avenue
Altadena, California

Dr. P. B. MacCready (50)
Mr. A. I. Weinstein (10)

Lockheed Aircraft Corporation
Missiles and Space Division
P. O. Box 504
Sunnyvale, California
ATTN: Mr. Ledolph Baer
Dr. Boccious

Mr. B. N. Charles
Boeing Airplane Company
Aero-Space Division
P. O. Box 3707
Seattle, Washington

DISTRIBUTION (CONT'D)

EXTERNAL (CONT'D)

Mr. Clemet Schmidt	Director (2)
Structure Branch	NASA-Flight Research Center
Aeronautical System Division	Box 273
Flight Dynamics Laboratory	Edwards, California
Wright Patterson AFB, Ohio	
	Dr. Hans A. Panofsky
Lt/Col. H. R. Montague	Department of Meteorology
Detachment 11, 4th Weather Group	Pennsylvania State University
Base Weather Station	University Park, Pennsylvania
Patrick Air Force Base, Florida	
Douglas Aircraft Corporation	
S-IV Project Director (2)	
THRU: MSFC Saturn Systems Office	
North American Corporation	
S-II Project Director (2)	
THRU: MSFC Saturn Systems Office	
Director	
Missile Meteorology Division	
U. S. Army Electronics Research and Development Activity	
White Sands Missile Range, New Mexico	
Director	
National Center for Atmospheric Research	
Boulder, Colorado	
Dr. Arnold Court	
Atmospheric Physics Group	
Physical and Life Science Laboratory	
Lockheed Aircraft Corporation	
Burbank, California	
Director (2)	
NASA-Lewis Research Center	
21000 Brookpark Road	
Cleveland, Ohio	